Imaging of Nonneoplastic Chest Wall Pathologies

19

Justin Stowell and Santiago Martínez-Jiménez

Abstract

The chest wall is commonly affected by nonneoplastic conditions including traumatic, infectious, arthritic, metabolic, and congenital lesions. Imaging plays a critical role in differentiating among these entities and other neoplastic mimics. Multimodality imaging evaluation including radiography, ultrasound (US), computerized tomography (CT), nuclear medicine, and magnetic resonance imaging (MRI) allows comprehensive evaluation of chest wall lesions and other ancillary findings. The radiologist plays an important role and is often be the first to identify abnormalities and alert clinicians and surgeons of both surgical and nonsurgical conditions. Thoracic surgeons and radiologists should work jointly in arriving at the imaging diagnosis and collaborate in the preoperative evaluation of patients who suffer from these conditions.

Keywords

Chest wall · Trauma · Hematoma · Fracture · Flail chest · Dislocation · Infection · Osteomyelitis · Septic arthritis · Inflammatory arthritis · Cellulitis · Abscess · Necrotizing fasciitis · Congenital chest wall disorders · Pectus excavatum · Osteoporosis · Renal osteodystrophy

Abbreviations

CT	Computed tomography
HIV	Human immunodeficiency virus
HU	Hounsfield unit
IV	Intravenous
MRI	Magnetic resonance imaging
SC	Sternoclavicular
TB	Tuberculosis
US	Ultrasound

19.1 Trauma

Imaging plays a critical role in the evaluation and management of patients after chest trauma. Documentation of the extent of thoracic injury (extrathoracic and intrathoracic) is not only helpful to direct appropriate treatment but also provides prognostic information [1]. Risk factors for increased morbidity and mortality in the blunt chest trauma include advanced age (>65), three or more rib fractures, development of pneumonia, and preexisting chronic lung disease [2]. Delayed

J. Stowell (✉)
University of Missouri-Kansas City School of Medicine, Kansas City, MO, USA

S. Martínez-Jiménez
Saint Luke's Hospital of Kansas City & University of Missouri-Kansas City School of Medicine, Kansas City, MO, USA

M. Anzidei, M. Anile (eds.), *Diagnostic Imaging for Thoracic Surgery*,
https://doi.org/10.1007/978-3-319-89893-3_19

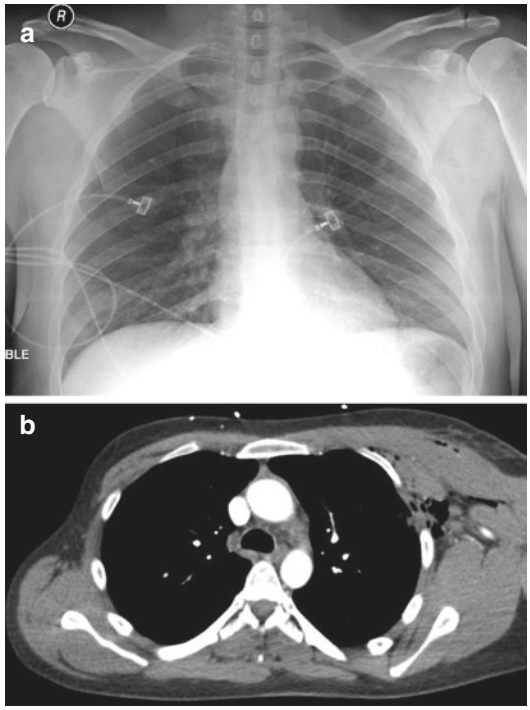

Fig. 19.1 Portable anteroposterior chest radiograph (**a**) and contrast-enhanced CT (**b**) demonstrate the superior sensitivity and specificity of CT for detailing the extent of chest wall injury after blunt and penetrating trauma. The patient suffered a stab wound to the left anterior chest wall, which caused left chest wall hematoma, subcutaneous air, and left pectoral laceration. Left upper lobe laceration and pneumothorax were also seen using lung windows on the chest CT (not shown), but were only subtly present on radiography

Table 19.1 Relative utility of commonly used imaging modalities in evaluation of the chest wall

Modality	Pros	Cons
Chest radiography	Readily available Fast and cost effective Prognostic value	Limited sensitivity for rib fractures and pneumothorax
Chest CT	Fast scan times Multi-planar imaging capabilities High sensitivity for detection of rib fractures, pneumothorax, pulmonary contusion or laceration, as well as other solid-organ or vascular injury	Expensive Radiation exposure Time-intensive interpretation Risk of adverse effects of iodinated contrast administration
Ultrasound	Fast and portable Relatively inexpensive Can be performed by clinicians High sensitivity and specificity for identification of rib and sternal fractures, pleural effusion, or rib fractures Dynamic exam with confirmation of site of maximal tenderness	Lacks sensitivity for small pleural space collections Limited for evaluation of scapular injuries Poor tissue penetration in obese patients or women with large breasts

complications related to blunt chest trauma include occult pneumothorax or hemothorax.

Chest radiography is important as the initial imaging assessment in patients after trauma. Since chest radiography is readily available and rapidly performed, it allows identification of common life-threatening thoracic injuries that require immediate intervention (e.g., pneumothorax, hemothorax). Further, radiographic findings often prompt additional imaging evaluation with chest CT, which has better sensitivity and specificity for chest wall, vascular, and visceral traumatic injuries, and often alters initial management [3] (Fig. 19.1). The utility of various imaging modalities in the initial evaluation of blunt chest trauma is presented in Table 19.1 [2]. It is generally recommended that both symptomatic and asymptomatic patients who sustain even minor blunt chest wall trauma return for follow-up chest radiographs 2 weeks after injury to exclude delayed complications.

19.1.1 Osseous

19.1.1.1 Sternal, Rib, and Costochondral Fractures

Sternal fractures are found in 8–10% of patients who sustain blunt chest wall injury [3–6]. The combination of sternal, scapular, or rib fractures and associated sternoclavicular joint dislocation comprises the "seat-belt syndrome" of motor vehicle collisions, indicating an increased likelihood of internal organ injuries [3]. Some authors have concluded that isolated sternal fractures in the absence of cardiac injury or arrhythmia may be managed conservatively with surgery rarely required [2].

Chest radiography is insensitive for the initial detection of non-displaced sternal fractures [7], and lateral views of the sternum are seldom obtained in the trauma setting despite their increased sensitivity for fracture. Axial chest CT readily depicts displaced sternal fractures, as well as concomitant retrosternal hematoma or other associated injuries (e.g., acute traumatic aortic injury) [3].

Up to 50% of patients with blunt trauma exhibit rib fractures, most commonly involving the fourth through ninth ribs [6, 8]. Simple rib fractures are generally of no clinical consequence, but may be associated with more serious injuries such as pneumothorax, hemothorax, pulmonary contusion or laceration, great vessel injury, or solid-organ injury [1]. Unlike radiography, CT offers high sensitivity and specificity for detection of rib fractures, with the additional benefit of assessing other radiographically occult injuries [3].

Flail chest occurs in up to 20% of major trauma victims and is defined as greater than or equal to three segmental (greater than two fractures occurring in the same rib) or greater than five adjacent rib fractures, leading to paradoxical motion of the chest during respiration (Fig. 19.2). Paradoxical chest wall motion impairs adequate ventilation, which, in combination with lung injury, can progress to acute respiratory failure [6].

One challenge is the evaluation of radiographically occult costochondral fractures. While ultrasound has been proven to be very sensitive [8], it is usually not practical in the acute setting. In our practice, we routinely use coronal maximum intensity projection (MIP) reformations to assess for costochondral fractures (Fig. 19.3). Detection of this type of injury is important as it is associated with more serious injuries and entails increased mortality [9].

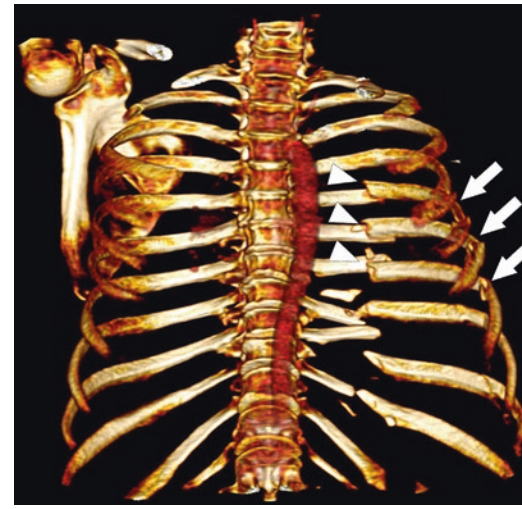

Fig. 19.2 Flail chest. Multilevel displaced segmental rib fractures (*arrows* and *arrowheads*) contributed to paradoxical chest wall motion during respiration and flail-chest physiology in this 70-year-old male who sustained a motor vehicle collision. 3D volume-rendered CT can be performed to better highlight the extent of thoracic injury and assist the thoracic surgeon in presurgical planning

Fig. 19.3 Costochondral fractures. Coronal CT with maximum intensity projection (MIP) reformations more readily depicts radiographically occult though clinically significant costochondral fractures (*arrows*)

19.1.1.2 Clavicle Fracture

Clavicle fractures represent up to 5% of all fractures. When describing a clavicular fracture, it is important to include the location (middle, distal, or proximal), degree of comminution or displacement, and likelihood of ligamentous injury [10]. Most (69–72%) clavicle fractures are mid-shaft in location, with distal and medial clavicle fractures representing 28% and 2–3% of the remaining fractures, respectively. Most clavicle fractures are non-displaced and extra-articular and can be managed conservatively. However, medial, posteriorly displaced fractures or associated sternoclavicular (SC) joint dislocations may cause injury to the great vessels, airway, or nerves within the superior medi-

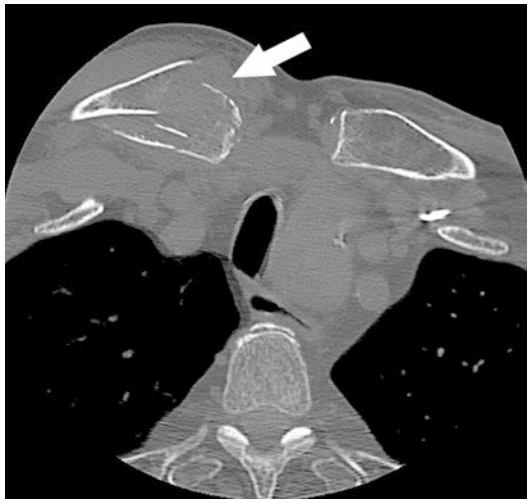

Fig. 19.4 Clavicle fracture. A CT from a 68-year-old man who sustained a comminuted, mildly displaced medial right clavicular fracture with surrounding hematoma (*arrow*) after an all-terrain vehicle rollover highlights the importance of cross-sectional imaging in characterizing radiographically occult chest wall injury

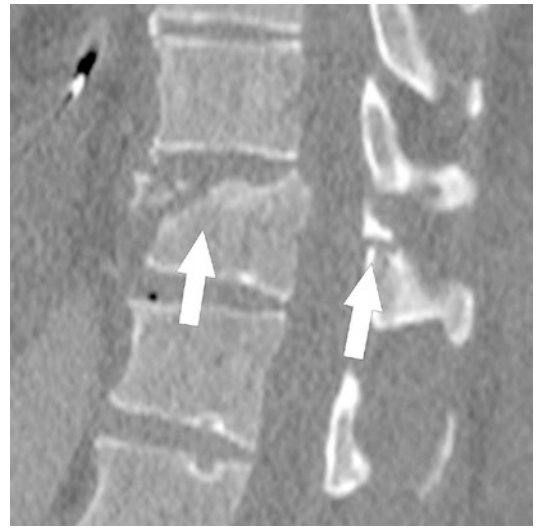

Fig. 19.5 Coned-down sagittal CT reveals a flexion-distraction "seat-belt" pattern of injury at T11. Fractures of the vertebral body (Chance fracture) and spinous process of T11 indicate simultaneous anterior column compression and posterior column interspinous ligament avulsion injuries, respectively (*arrows*). This pattern has a high association with coexistent abdominal and spinal cord injuries

astinum and often have surgical implications. Most of these are radiographically occult and are best characterized on axial CT (Fig. 19.4). Multiplanar reformatted images and 3D reconstructions may be helpful to the surgeon in preoperative planning.

19.1.1.3 Scapular Fracture

Because it is relatively protected by surrounded shoulder girdle and back musculature, the scapula is rarely injured in blunt trauma. The presence of scapular injury should raise suspicion for more extensive thoracic injury. Most scapular fractures are managed conservatively in the absence of involvement of the glenoid or scapular neck [6].

19.1.1.4 Spinal Trauma

The thoracic spine should be carefully evaluated in the setting of blunt chest trauma, as injuries in this region can be complicated by devastating neurologic defects in up to 60% of patients [6]. Vertebral body (wedge, burst, and Chance-type) is typically located near the thoracolumbar junction [5, 6]. Wedge fractures typically spare the posterior aspect of the vertebral body. Burst fractures involve the posterior aspect of the vertebral body, which entails increased risk of cord injury. Finally, Chance fractures are defined by extension into the posterior elements or ligamentous structures. CT defines the extent of injury, including pedicle and spinous processes fractures, as well as paraspinal hematoma (Fig. 19.5). CT may also provide information of the integrity of the spinal canal and neural foramina. MRI is often required to assess for spinal cord injury, which may be present in up to 30% of traumatic spine injuries especially in the setting of burst and Chance fractures [11].

19.1.2 Joints

19.1.2.1 Sternoclavicular and Manubriosternal Dislocation

Lateral compression injuries with medially directed force through the shoulder may lead to sternoclavicular dislocation. Patients present with anterior chest wall tenderness, impaired shoulder range of motion, and often visible deformity at the sternoclavicular joint. The direction of dislocation of the medial clavicular head in relation to the manubrium has prognostic implications. Most SC dislocations are anterior, with posterior dislocations less common but associated with worse prognosis as they are frequently associated with mediastinal injury (e.g.,

head/neck vessels and tracheal compression) [6]. SC dislocation is often occult on radiography; however, it may occasionally be seen as abnormal position of the clavicular head. CT readily demonstrates anterior or posterior position of the medial clavicle and allows for detailed assessment of the adjacent mediastinal structures [12] (Fig. 19.6).

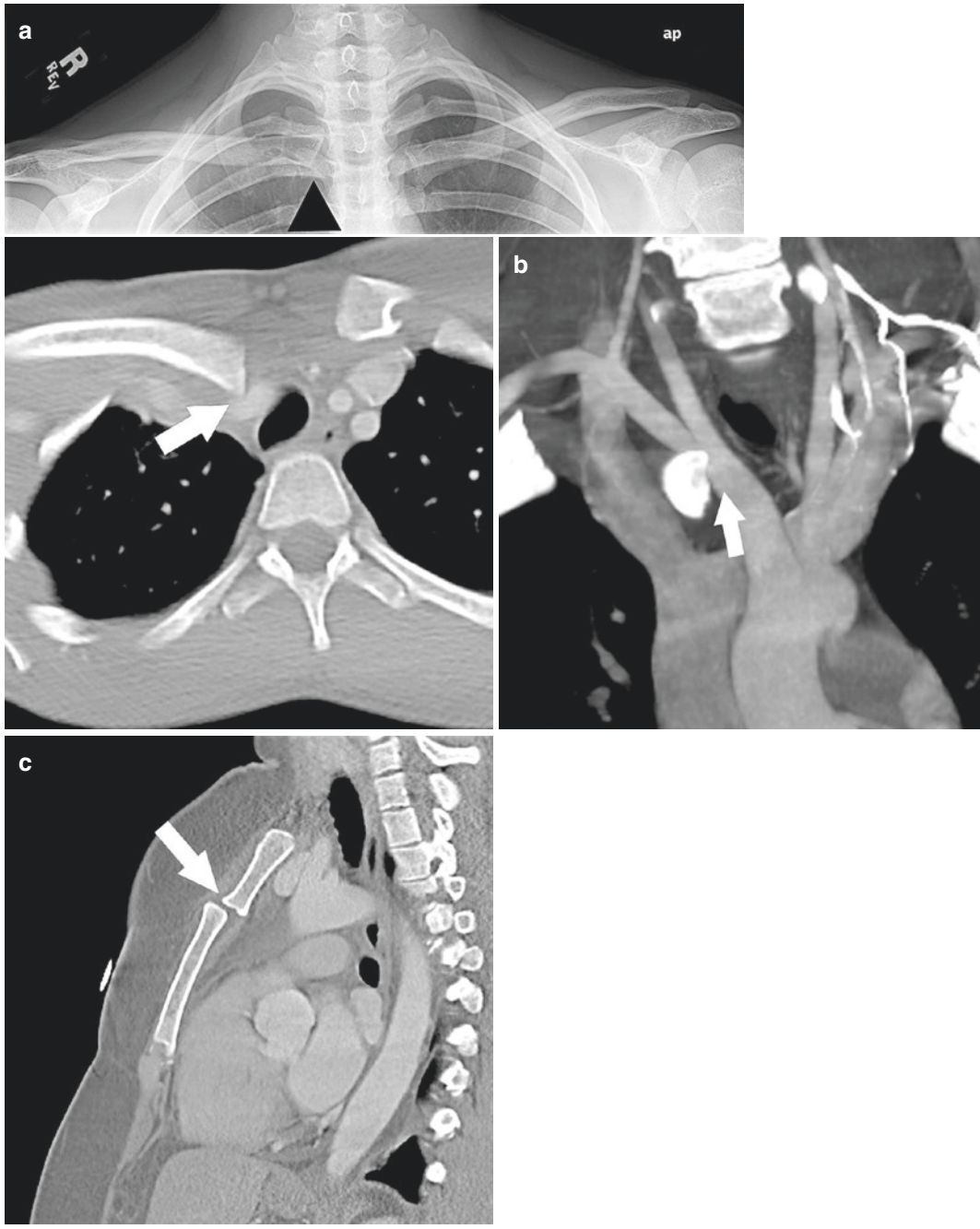

Fig. 19.6 Sternoclavicular and manubriosternal dislocation. (**a**) Chest radiograph shows subtle asymmetric displacement of the medial right clavicle (*black arrowhead*). Contrast-enhanced axial (**b**) and coronal MIP (**c**) CT better characterizes the posterior displacement of the medial clavicle with compression of the right brachiocephalic artery (*arrows*). (**c**) Sagittal CT is best to characterize the degree of displacement in manubriosternal dislocations (*arrow*). Manubriosternal dislocations are rare and imply high-force injury mechanisms

Manubriosternal dislocation is rare, occurring most frequently in the setting of trauma or exaggerated kyphosis related to chronic diseases (e.g., osteoporosis and rheumatoid arthritis). Dislocations are classified as either type 1 or type 2 based on the posterior or anterior position of the sternum in relation to the manubrium, respectively [12].

19.1.2.2 Costovertebral Fracture-Dislocations

Costovertebral dislocations involve ligamentous or osseous disruption of the costocentral and costotransverse constituents of the arthrodial joint structure. The costocentral joint spans a large portion of the posterolateral disk space. It is stabilized by a thin synovial capsule and ligaments (interarticular and radiate), which may not be visualized on CT. Costovertebral joints are comprised primarily of two thick ligaments which stabilize the neck and tubercles of the ribs to the transverse processes, oriented in a transverse plane. Collectively, these joints provide important stabilization and support to the thoracic spine [13].

While uncommon, costovertebral joint injuries are often overlooked as they are generally radiographically subtle. Their presence suggests serious radiographically occult injuries of the chest and thoracic spine and should be further evaluated with cross-sectional imaging. Costocentral articulations are well defined on chest radiographs, where the costal head can be seen articulating with the vertebral pedicle. The joints are best evaluated in the axial plane on CT bone window settings. While traumatic costovertebral fracture-dislocations are most common, dislocation with penetration of the rib into the spinal canal or neuroforamen may be seen in patients with scoliosis or neurofibromatosis [13, 14].

19.1.3 Soft Tissues

19.1.3.1 Direct Injury

Blunt and Penetrating Trauma

Direct muscle and soft-tissue injury results in hemorrhage that ranges from intramuscular interstitial bleed to frank hematoma. Additionally, penetrating trauma (e.g., stab wounds) may disrupt the muscle fibers and result in denervation atrophy.

Hematomas may be the result of arterial (intercostal, internal mammary, or subclavian artery) or venous bleeding. Extrapleural hematomas collect between the endothoracic fascia and parietal pleura, which on CT appear as a convex, hyperdense collection with characteristic displacement of the extrapleural fat from the chest wall with mass effect on the adjacent lung [5]. Occasionally, sites of active bleeding may be detected if intravenous contrast is utilized; this may be facilitated by using MIP reformations. Subcutaneous fat stranding is another common finding. Acute hemorrhage is typically hyperdense, and the affected musculature may be focally enlarged. CT is helpful to detect radiographically occult injuries which include pneumothorax (15%), hemothorax (11%), and combined hemopneumothorax (9%), as well as hemopericardium [15] (Fig. 19.1).

Hematomas have variable appearance on MR, depending on the extent and age of the blood products (Table 19.2). Fat-suppression

Table 19.2 Variability of imaging features in chest wall soft-tissue injury

Classification	MRI appearance
Type 1 (seroma)	Homogenous hypointense T1, hyperintense T2; no capsule formation
Type 2 (subacute hematoma)	Homogenous hyperintense T1 (methemoglobin) and T2, becoming heterogeneous with time; +/− hemosiderin capsule; +/− internal fat, fluid–fluid levels, or septations; patchy enhancement from neovascularity
Type 3 (chronic organizing hematoma)	Hypointense T1 and heterogeneous hypo- to isointense T2 signal; internal enhancement from neovascularization and granulation tissue; hypointense ring from hemosiderin and fibrous pseudocapusle
Type 4 (closed laceration)	No capsule; T1 hypointense, T2 hyperintense, variable enhancement
Type 5	Pseudonodular appearance with variable T1 and T2 signal; variable internal or peripheral enhancement
Type 6 (infected hematoma)	Thick enhancing capsule +/− sinus tract formation

techniques distinguish fat from subacute blood product on T1-weighted images. Hematomas typically resolve in 6–8 weeks after injury.

Soft tissues occasionally react to blunt trauma by the formation of a circumscribed mass of granulation tissue which may eventually form new bone (heterotopic ossification) due to activation of osteoblast progenitor cells in damaged tissue. Radiography and CT vary in time, progressing from early nonspecific soft-tissue swelling (0–2 weeks) to heterogeneous soft-tissue enhancement and periosteal reaction in adjacent bone with formation of amorphous osteoid (3–4 weeks). Beyond 6 weeks, a characteristic zoning phenomenon occurs wherein mature cortical bone forms around the periphery of the immature osteoid centrally [16]. MR imaging features also evolve over time from injury, manifesting initially as heterogeneous increased T2 signal (edema), with progression to an enhancing mass-like high T2 signal intensity lesion which mimics a soft-tissue sarcoma. In many cases, patients may be referred to the thoracic surgeon for suspicion of underlying tumor. With increasing age of injury beyond 6–8 weeks, peripheral ossification begins, leading to low signal on T1- and T2-weighted images, as well as dark signal on gradient echo sequences [16, 17] Unlike sarcomas, the overall lesion of heterotopic ossification tends to decrease in size over time.

19.1.3.2 Indirect Injury

Muscle Strain and Tendon Injury

Musculotendinous injury (muscle strains, ruptures, and hematoma) occurs most frequently in active individuals, with higher risk in weightlifters, football players, and wrestlers [4]. Pectoralis major is by far the most commonly injured chest wall muscle, followed successively in frequency by pectoralis minor, internal oblique, or external oblique. Muscle strains represent either partial or complete tears of the muscle fibers at the musculotendinous junction, often resulting from sudden forceful loads applied during eccentric contraction. Most indirect muscle injuries are not imaged and may be conservatively managed. Imaging appearance of indirect muscle injury is dependent on the grade of injury.

Ultrasound may be used in the evaluation of musculotendinous injury, manifesting as hypoechoic signal or non-visualization of a tendon and loss of the normal fibrillary pattern. In full-thickness tendon tears, a gap may be seen in the disrupted tendon with a blunt-ending, retracted tendon fragment, which may produce a refractive shadow. Adjacent fluid collections or hematomas may also be seen. Imaging features of muscle injury are identical to other soft-tissue hematomas, with progressive liquefaction of the blood product over the healing process. Once liquefied, the collection may undergo ultrasound-guided aspiration.

CT is inferior to MRI and US in characterization of soft-tissue injury. CT may show ill-defined heterogeneous density near the insertion or origin of the involved muscle, with varying degrees of perimuscular fluid or hemorrhage. Bony avulsion fractures may be detected using bone windows. MRI readily depicts all degrees of traumatic soft-tissue injury.

19.2 Infection

Primary spontaneous infection of the chest wall is rare but may occur in the certain scenarios such as altered immunity, intravenous drug abuse, diabetes mellitus, or previous trauma or surgery [18]. Secondary chest wall infections (i.e., osteomyelitis) are usually related to pulmonary or pleural infections (e.g., *Actinomyces*, tuberculosis, or fungal infection, discussed subsequently) or recent surgery (e.g., sternotomy). *Staphylococcus aureus* and *Pseudomonas aeruginosa* are the organisms most commonly responsible for pyogenic infection of the chest wall. *Salmonella* species may be responsible for chest wall infections in a subset of patients (i.e., sickle cell) [19]. Imaging is integral to evaluation, as clinical and laboratory evaluations are often nonspecific. Despite inherent limitations in evaluation of the chest wall, chest radiography is often the first modality employed. CT and MRI provide better detail of the extent of infection, as well as vital anatomic information related to bone destruction (CT) and soft-tissue complications (MR). Cross-sectional imaging is a necessary component of

presurgical planning prior to chest wall resection. Furthermore, CT and ultrasound may be utilized in drainage procedures or percutaneous biopsy.

19.2.1 Osseous

19.2.1.1 Osteomyelitis

Pyogenic Infection

Osteomyelitis is defined as infection of the bone and marrow space by various microorganisms. Primary chest wall infections are rare, with most occurring in the setting of diabetes, immunosuppression (chronic immunosuppressive therapy or HIV), or trauma (including surgery). Osteomyelitis of the sternum, ribs, clavicles, or spine occurs most commonly from contiguous spread of infection from pulmonary or pleural processes [19]. Hematogenous involvement may also occur in the setting of intravenous drug abuse, severe immune suppression (AIDS), hemoglobinopathies, and other immune-suppressed states [20]. Responsible organisms in pyogenic osteomyelitis most commonly include *Staphylococcus aureus* and *Streptococcus* species. However, other organisms may be implicated in particular populations (Table 19.3) [18–23]. Early recognition and initiation of treatment are important to prevent progression of infection to subacute or chronic stages, and to prevent complications of sepsis.

Osteomyelitis is characterized histologically by marrow edema and cellular infiltration, with contiguous intramedullary spread of infection via Haversian and Volkmann canals, leading to eventual cortical destruction and spread to adjacent soft tissues or joints [20]. Intramedullary pressures increase with cellular proliferation and progressive edema, which may lead to intramedullary vascular compromise, ischemia, and necrosis. Over time, the bone may react by activation of osteoclasts and formation of sclerotic bone in an attempt to sequester or wall off the offending organism, producing an interosseous abscess and eventual sequestrum.

Primary sternal osteomyelitis is uncommon. Sternal and rib osteomyelitis typically occur as complications of recent trauma, surgery, or contiguous chest wall or mediastinal infection. Postoperative sternal osteomyelitis is associated with a mortality rate as high as 50% [22] and should be aggressively treated. While radiography is often insensitive, CT highlights osseous destruction, erosion, periosteal reaction, and soft-tissue abscess (Fig. 19.7). Pyogenic infections tend to involve the opposing ends of the rib, at the costochondral and costovertebral junctions [22] (Fig. 19.8). MRI has high sensi-

Table 19.3 Implicated organisms in chest wall infections affecting particular patient populations

Patient condition	Associated organisms
Immunocompetent	*Staphylococcus aureus, Streptococcus pyogenes*
IV drug abusers	*Pseudomonas aeruginosa*
Median sternotomy	*Staphylococcus aureus, Pseudomonas, Serratia, Klebsiella*
HIV and AIDS	Usual bacterial organisms, *M. tuberculosis*, *Nocardia*
Lung or heart transplant	Fungal (*Aspergillus*, *Actinomyces*, *Blastomyces*)

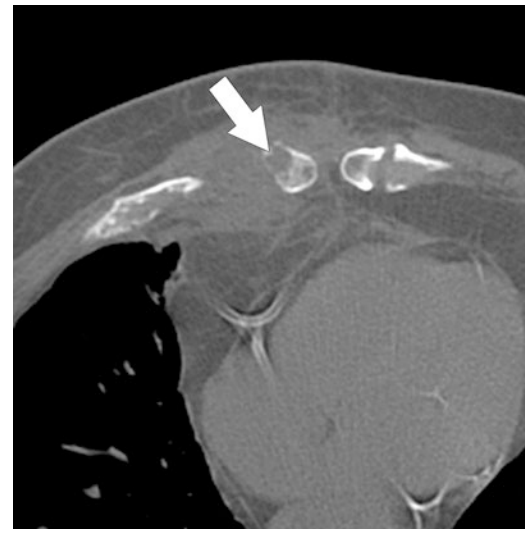

Fig. 19.7 Sternal osteomyelitis extending into the anterior mediastinum after median sternotomy. CT depicts sternal erosion (*arrow*) and the extent of surrounding phlegmon in a patient who had recent sternotomy for coronary artery bypass graft surgery. CT is the preferred modality for evaluating complications of sternal osteomyelitis, which include mediastinitis and abscess

tivity for early marrow edema and characterizes abscesses or fistulae. The radiologic findings of more extensive infection are nonspecific and overlap with other entities such as plasmacytoma and metastases. Therefore, clinical context and histologic correlation is required.

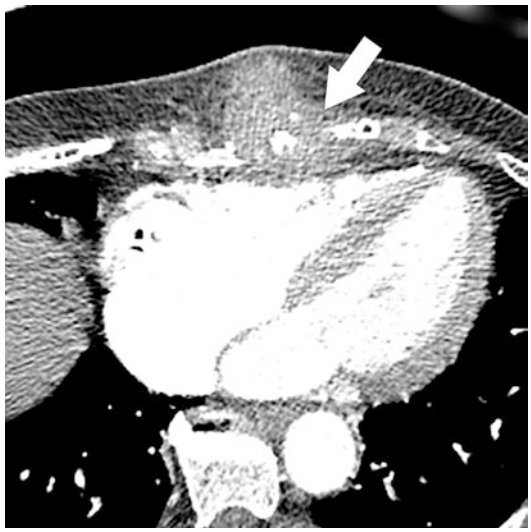

Fig. 19.8 Costochondral osteomyelitis. Extensive soft-tissue inflammation surrounds an area of costochondral and rib destruction (*arrow*) from contiguous spread of pyogenic infection after recent sternotomy

Multi-modality imaging is often required when osteomyelitis is clinically suspected [20]. Radiographic findings include soft-tissue swelling and thickening of septae in subcutaneous fat (edema), often before osseous changes are present. Air-fluid levels in the soft tissues may indicate abscess [18]. Osseous changes include cortical erosion or sclerosis, osseous destruction, and periosteal reaction, which generally suggests that the infection has been present for 1–2 weeks. Regional hyperemia and marrow infiltration will lead to localized osteoporosis and eventual trabecular destruction/osteolysis [20]. Normal radiographs do not exclude the presence of osteomyelitis.

MRI is the most sensitive and specific modality for detection of early osteomyelitis, ranging from 82 to 100% and 75 to 96%, respectively [20, 24]. Fat-suppressed T2-weighted and short tau inversion recovery (STIR) sequences are sensitive to the presence of marrow edema, manifesting as areas of hyperintensity (Figs. 19.9 and 19.10). Replacement of the normal hyperintense signal of marrow fat on T1-weighted sequences

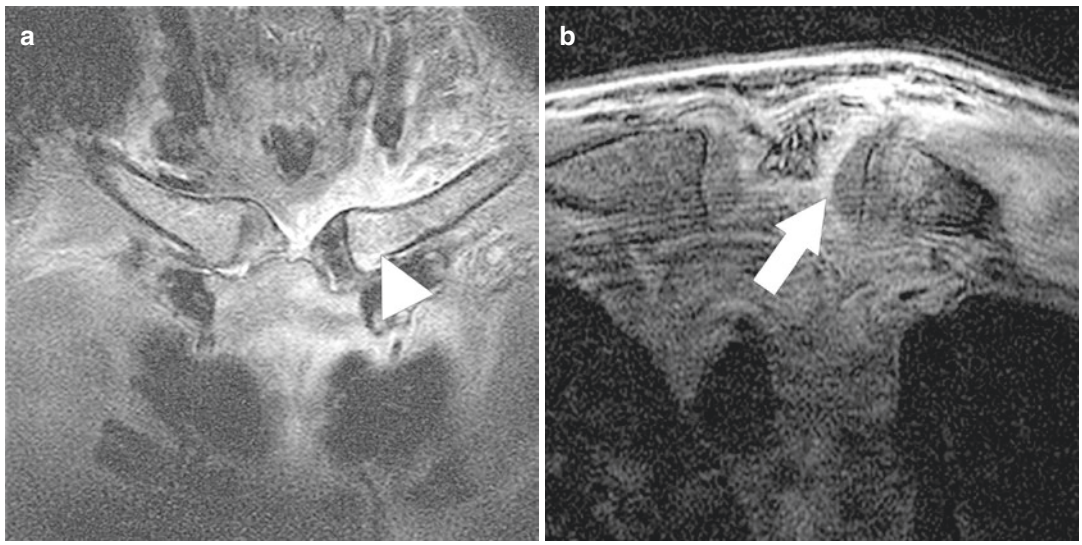

Fig. 19.9 Sternoclavicular septic arthritis. (**a**) Coronal short tau inversion recovery (STIR) MR reveals expected periarticular inflammation and clavicular marrow edema (*arrowhead*) surrounding the left SC joint. (**b**) Axial T1 fat-suppressed MR after intravenous gadolinium contrast material shows corresponding enhancement of the left SC joint (*arrow*) and periarticular soft tissue

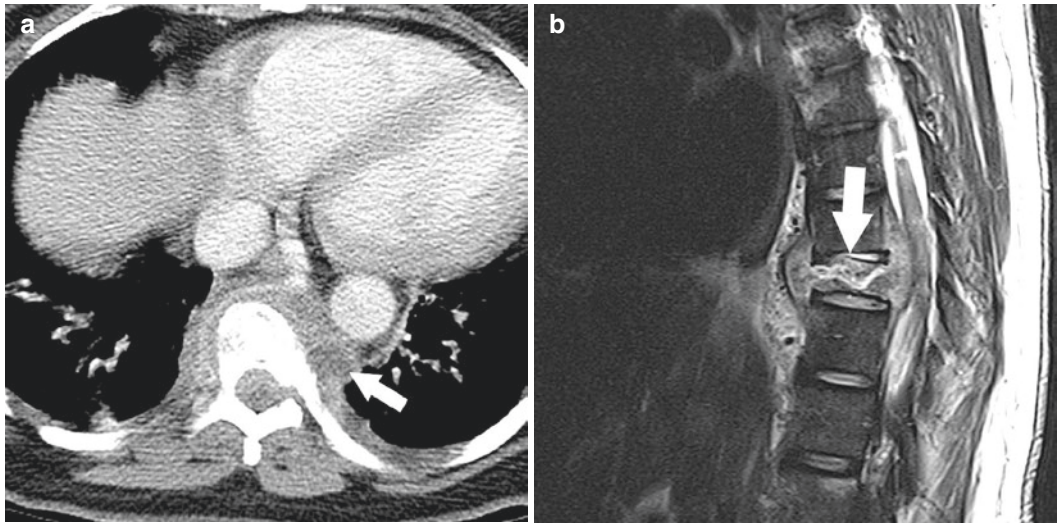

Fig. 19.10 Pott disease. (**a**) CT reveals low-attenuation paravertebral soft-tissue masses and fluid collections (*arrow*) in a young patient with spinal TB. Paravertebral masses are present in 95% of cases, often with calcification. Other CT findings include anterior endplate erosion without significant reactive sclerosis, and wedge deformities. (**b**) Sagittal MRI STIR sequence shows marrow edema as increased signal and a linear hyperintense cleft in the involved vertebral body (*arrow*), indicating a pathologic fracture. MRI STIR sequence also delineates the craniocaudal spread of the paraspinal infectious material, as well as anterior spread into the lower mediastinum. Marked cord compression is seen to better advantage with MRI

by intermediate to low signal indicates an infiltrative process. The clinician must be aware that imaging findings in acute osteomyelitis are nonspecific, as similar findings may be seen in noninfectious processes, including trauma, fracture, ischemia, and tumor [24]. MR features of the various stages of osteomyelitis are summarized in Table 19.4.

Despite its inferior sensitivity (73%) and specificity, scintigraphy may be considered as an adjunct modality, particularly for evaluating patients who have contraindications to MRI. Three-phase bone scans using technetium-99m-labeled methylene diphosphonate (MDP) reveal increased radiotracer uptake in arterial flow, blood pool, and 3-hour delayed imaging [20, 25]. The intensity of uptake localizes to the areas of infection. Specificity of bone scintigraphy is reduced in the presence of complicating conditions (i.e., trauma, surgery, orthopedic hardware, and diabetes). Other nuclear medicine techniques utilizing various radiopharmaceuticals (technetium-99m hexamethylpropylenamine oxime (HMPAO)-labeled white blood cells, murine immunoglobulin-M monoclonal antigranulocyte antibodies, or ciprofloxacin-labeled moi-

Table 19.4 Expected evolution of osteomyelitis on MRI

Stage of infection	MRI appearance
Acute: edema and exudate	Ill-defined low T1 signal High signal T2, STIR Ill-defined soft-tissue planes Disruption of dark cortical signal + enhancement Rim enhancement = abscess Intramedullary fat globules (marrow necrosis)
Subacute: intraosseous abscess formation	Low T1 signal surrounding abscess (granulation tissue) High T2 signal within abscess and in surrounding marrow (edema) "Double-line effect" or "target" appearance = concentric enhancing granulation tissue with low signal band of sclerosis and peripheral rim enhancement Cortical thickening
Chronic	Low T1 Low T2 (scarring and bony sclerosis) Sharp zone of transition between normal and infected marrow "Rim sign" = peripheral low signal on all sequences corresponds to fibrotic changes and reactive bone Areas of non-enhancement (devitalized bone, sequestrum) Cortical thickening +/− sinus tracts

eties) may also be considered [20, 24]. However, false-negative scans may occur in the setting of chronic or partially treated osteomyelitis.

Tuberculosis

The spine is the most common site of musculoskeletal *Mycobacterium tuberculosis* infection, also known as Pott disease [26] (Fig. 19.10). The thoracic spine is most commonly affected. The chest wall is affected in up to 10% of extrapulmonary TB [21]. Infections manifest with osteitis of the ribs, sternum, vertebrae, as well as costochondral and costovertebal articulations. A strong predilection for the sternal margins has been associated with TB, possibly a result of secondary infection from infected internal mammary chain lymph nodes [21, 27]. Nevertheless, the sternum is affected in less than 1% of all cases of tuberculous osteomyelitis [28]. Others report a predilection for the rib shaft (unlike pyogenic infection) with osseous destruction and adjacent abscess formation [22, 29]. Radiographs will be normal. Osseous changes (cortical erosions or expansile osteolytic mass) occur secondary to direct infection or pressure necrosis from inflammatory granulation tissues and are better depicted on CT and MR. Signs of bone repair (periosteal reaction or sclerosis) are less frequently seen in TB than in pyogenic osteomyelitis [22, 29]. Necrotic lymph nodes may form subpleural collections referred to as "cold abscesses," which can extend from the chest wall and ultimately require wide surgical resection in addition to multidrug therapy [21, 27]. Cutaneous fistulae may also develop [27, 30]. CT reveals expansile, destructive lytic lesions with adjacent sclerosis with nearby soft-tissue thickening and enhancement. The soft-tissue component often is in continuity with mediastinal or internal mammary lymphadenopathy [29]. Ultrasound and CT are useful for diagnosis and sampling.

Actinomyces

Of the five major forms of actinomycotic infections, the thoracic form is quite common (15%) [21, 22, 31]. *Actinomyces israelii* is a gram-positive anaerobic inhabitant of the oral cavity, which explains its predilection to involve the cervicothoracic and abdominal regions. Isolated actinomycotic chest wall infection is rare, and usually occurs secondary to a pulmonary infection. Aspiration of oral flora leads to parenchymal infection, with subsequent spread through the pleura and into the chest wall. Complications of actinomycosis infection include empyema and empyema necessitatis, chronic pleurocutaneous fistula, and systemic dissemination [21, 31]. Radiographic manifestations include nonspecific osteolysis with or without periostitis, or subpleural consolidations with or without pleural effusion [31, 32]. Bone scintigraphy may show focal radiotracer uptake in the region of bony involvement and periosteal new bone formation [31]. CT and MRI show to better advantage the extent of thoracic and soft-tissue involvement. Intravenous contrast highlights the enhancing inflamed tissue and rim-enhancing abscesses, if present [21, 31, 32]. MRI features include nonspecific T1 hypointense as well as T2 and STIR hyperintensity, often with enhancement [31]. Ultrasound of the chest wall may assist in diagnosis or drainage of soft-tissue abscesses (complex fluid collection with surrounding hyperemia), empyema, and soft-tissue mass, but generally underestimates the extent of disease.

Fungal and Hydatid Infection

Fungal organisms are rare but increasingly recognized sources of chronic infections of the ribs and sternum, especially in the setting of immunosuppression. Sternal osteomyelitis and costochondritis often result from hematogenous dissemination or contiguous spread of pulmonary infections. Costal cartilages, especially after perichondrial damage, are particularly susceptible to infection. While *Aspergillus* infection as a complication of surgery is well described, primary *Aspergillus* infections occur in the setting of immune compromise (diabetes, alcoholism, prolonged antibiotic therapy, immunosuppressive therapy, neutropenia, and HIV) or IV drug abuse [23, 33]. Other fungal infections (histoplasmosis, blastomycosis, cryptococcosis, and coccidioidomycosis) are rare, occurring most often in the immunocompromised patient, and share similar imaging features. Radiographic manifes-

tations include nonspecific osseous destruction and soft-tissue masses [22]. Histocytopathologic sampling must confirm the diagnosis. Treatment often requires radical debridement of chronically inflamed tissues, with potential necessity of chest wall defect reconstruction [21, 22, 33].

Hydatidosis represents human parasitic infection with the larval form of the *Echinococcus granulosus*. Although rare in the United States, the parasite is very common among rural populations in Mediterranean countries, Australia, and South America, with increasing incidence in China [34]. Both costovertebral and primary rib hydatidosis have been described with rib involvement in 22–72% of cases [22, 34]. Radiographic manifestations include a permeative, multiloculated expansile predominantly lytic bony destruction, adjacent soft-tissue swelling, and pleural thickening. Periosteal new bone formation and sclerosis are uncommon. Calcified extraosseous cysts may be present in over 1/3 of cases. Ultrasound may be helpful to determine cystic appearance of lesions. CT and MRI are useful in presurgical planning, showing extraosseous disease and potential spinal involvement. The MRI appearance of the cysts includes hyperintense T1 (high protein content) and T2 signal. Daughter cysts may be less proteinaceous, manifesting with lower T1 and higher T2 signal. There is faint, thin cyst wall enhancement after gadolinium contrast administration. Histologic confirmation must exclude other mimics including metastasis, plasmacytoma, aneurysmal bone cyst, or cystic neurogenic tumors. Treatment typically involves radical surgical resection to avoid recurrence or inadvertent cyst rupture. Cyst rupture may lead to dissemination of infection or even anaphylaxis, and thus needle biopsy is contraindicated [22, 34, 35]. However, in poor surgical candidates, percutaneous needle aspiration of cyst contents with injection of antiprotoscolicidal has been described [34].

19.2.2 Joints

19.2.2.1 Primary septic arthritis

Septic arthritis is defined by direct invasion of microorganisms into the joint space. Sternoclavicular joints comprise only 2% of all pyogenic arthritis, but are frequently complicated by periarticular abscess because of the capsule limitations to distention [36]. The joint may become secondarily affected by spread of infection from adjacent sternal osteomyelitis or mediastinal abscess [37]. Most pyogenic SC joint infections are unilateral, with slight predilection for the right side. Primary manubriosternal infections occur almost exclusively in the setting of IV drug abuse, and share similar imaging features. Close anatomic relationship of these joints to the pleural space, mediastinum, and great vessels explains associated infectious involvement of vital structures. The superficial location of the joints allows for easy palpation to elicit physical findings of focal tenderness, cutaneous erythema and induration, and joint capsular swelling. Referred pain to the shoulder may be found in 25% of cases. Surgical intervention (incision and drainage, debridement, or en bloc chest wall resection) is indicated in the presence of failed antibiotic therapy, periarticular fluid collections/abscess, and osseous destruction.

Cross-sectional imaging is the cornerstone of diagnosis and should be performed routinely in all cases of suspected SC joint septic arthritis to confirm the diagnosis and determine possible complications, especially the presence of retrosternal or mediastinal abscess [36]. CT findings include periarticular inflammation, osseous erosion, sclerosis, and periosteal reaction of the surrounding bone (Fig. 19.9). However, osseous changes may not be apparent at early stages (i.e., first 1–2 weeks). Degenerative changes of the joints can simulate infection on radiography, but CT findings of periarticular osteophytes, subchondral sclerosis, and occasional intra-articular gas in the absence of soft-tissue inflammation are essentially diagnostic [22]. Radiographs and ultrasound findings may be absent despite the presence of SC joint infection. Ultrasound may readily characterize periarticular soft-tissue fluid collections (joint effusions, abscess), synovial thickening and hyperemia (synovitis), and presence of soft-tissue collections [22, 38]. MRI can detect early inflammatory changes of bone, joint, and soft tissues, depicted as heterogeneous low

T1 signal and high signal intensity (edema) on T2-weighted sequences. Intravenous gadolinium further characterizes inflamed soft tissues and can outline areas of non-enhancing, devitalized tissue [22] (Fig. 19.9).

SC joint infections with atypical organisms are rare and exhibit unique clinical and imaging manifestations. Nearly 3% of TB extraspinal arthritis involves the SC joint, manifesting with extensive osteolysis, periarticular inflammatory soft-tissue mass, abscess with rim enhancement and mural calcifications, and lack of periosteal reaction in adjacent bone [22]. Manubriosternal joint involvement is very rare [39]. US and CT may reveal bony sequestra within areas of smoldering osteolysis. Radiography is insensitive and nonspecific, and may demonstrate the presence of a presternal soft-tissue mass with or without osseous changes. Most systemic infections with *Brucella* involve the musculoskeletal system, and 2–5% affect the SC joint. Most brucellar SC joint infections are treated with long-term antibiotic therapy, and surgical control is seldom necessary. CT may show subchondral erosion and joint space enlargement. Healing changes include bony sclerosis and new bone formation [22, 29].

In the setting of chronic relapsing sternoclavicular inflammation, hyperostosis, and osteitis, a common mimicker of pyogenic SC arthritis—synovitis, acne, pustulosis, hyperostosis, and osteitis syndrome (SAPHO)—should be raised. SAPHO is an inflammatory disorder of the skin and musculoskeletal system, occurring in otherwise healthy young adults in the absence of immune suppression or infectious etiology. The sternoclavicular joints are involved in 60–90% of cases, with concomitant sacroiliitis and spondylitis [22]. Cultures from joint aspiration and bone biopsies may be negative or may isolate *Propionibacterium acnes*, and patients may have undergone treatment with prolonged antibiotics and prior surgical debridement. Sternocostoclavicular hyperostosis (Fig. 19.11), along with erosion, subchondral sclerosis, and ankylosis, is a radiologic and CT feature. T2-weighted MR sequences additionally may reveal active marrow edema [12]. Classically, technetium-99m bone scintigraphy reveals uptake in the sternocostoclavicular and manubriosternal joints in a highly specific "bulls horn" configuration [40] (Fig. 19.11). CT and MRI features are nonspecific and do not reliably differentiate SAPHO-related osteitis and hyperostosis from those of other infectious etiologies. Nonsteroidal anti-inflammatories (NSAIDs) are the mainstay of treatment. Surgical intervention is rarely indicated.

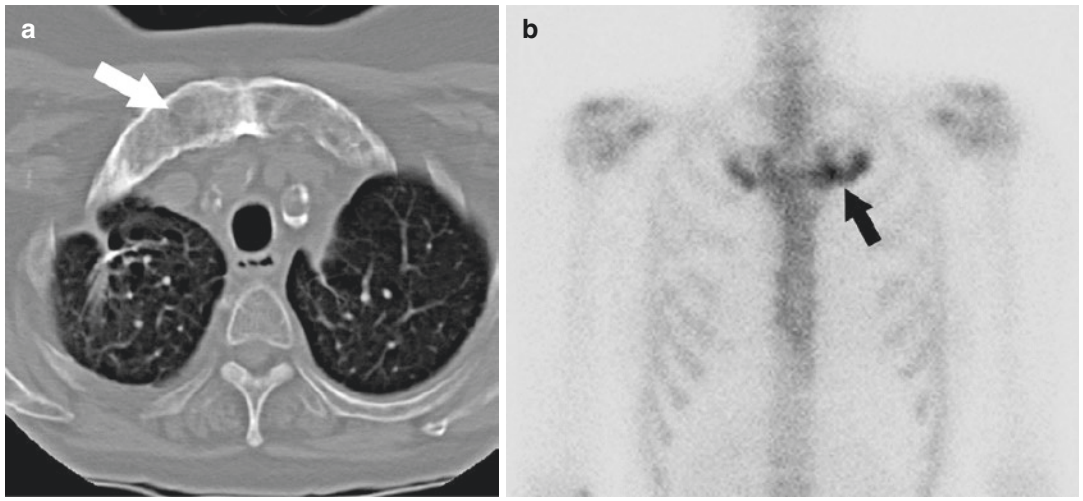

Fig. 19.11 Synovitis, acne, pustulosis, hyperostosis, and osteitis syndrome (SAPHO). (**a**) CT shows hyperostosis, expansion, and ankylosis of the sternoclavicular joints (*arrow*). (**b**) Technetium-99m bone scan in the same patient manifests the classic "bull's horn" appearance of increased radiopharmaceutical uptake in the involved sternoclavicular joints (*arrow*)

19.2.3 Soft Tissues

19.2.3.1 Cellulitis, Pyomyositis, and Abscess

Cellulitis refers to an infection of the dermis and subcutaneous fat related to bacterial inoculation from small traumatic defects in the skin; contiguous spread from adjacent infected bones or joints; or hematogenous spread. Recurrent cellulitis may occur in the setting of postoperative vascular and lymphatic damage (e.g., breast surgery or lymph node dissection), intravenous drug abuse, or radiation therapy. Clinical presentation includes fever and malaise with warm, tender, erythematous areas of skin. Extreme cases may manifest with edema, pustules, vesicle and bulla formation, necrosis, or lymphangitis. Common causative microorganisms in the immunocompetent adult patient are *Staphylococcus aureus* or *Streptococcus pyogenes*. Anaerobes should be considered in patients with peripheral vascular disease, venous insufficiency, or diabetes. In the setting of immunosuppression (e.g., diabetes, HIV, long-term corticosteroid therapy, neutropenia, leukemia), the concern for infection with atypical or opportunistic organisms (e.g., *Nocardia*, *Cryptococcus*, or atypical mycobacteria) should be raised. While most cases can be managed medically, some patients may require surgical debridement [41].

The full extent of cellulitis is best characterized with MRI given the sensitivity of MR in depicting high T2 signal (edema) within the involved subcutaneous tissues. On T2-weighted images, a lacelike reticular pattern of hyperintense signal is often present in the subcutaneous fat [4, 42]. Small fluid collections and variable tissue enhancement can be seen after intravenous gadolinium. MRI may characterize involvement of deeper chest wall structures (e.g., muscles, joints, bones, or even pleura and lung) [4].

Bacterial infection of skeletal muscle (i.e., pyomyositis) is increasing in incidence, especially in susceptible populations (e.g., patients with diabetes or HIV). Responsible organisms are similar to those seen in cellulitis. CT and MRI reveal muscle enlargement, edema, enhancement, and frequently intramuscular abscess formation [4] (Fig. 19.12).

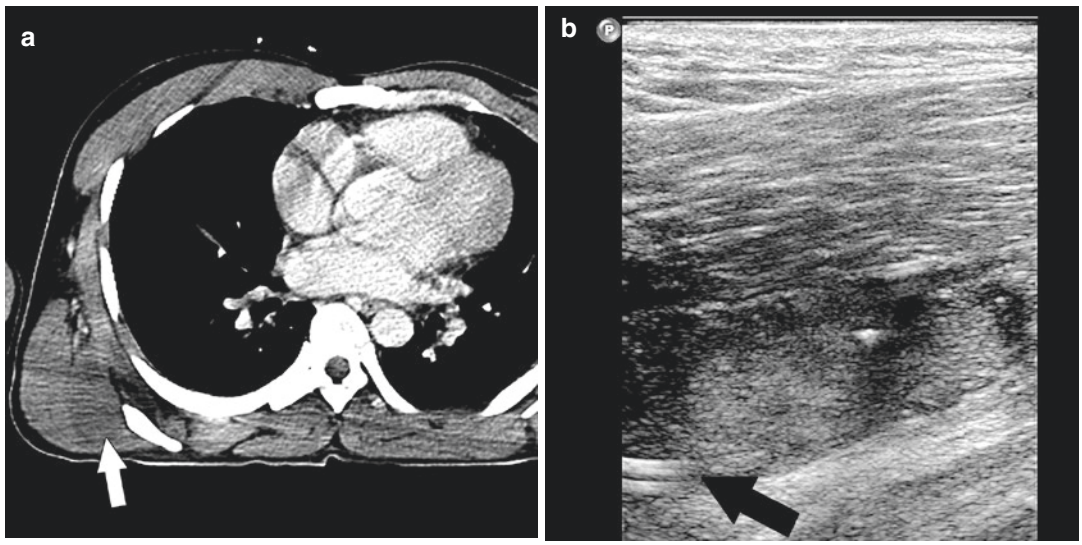

Fig. 19.12 Pyogenic intramuscular abscess. A 34-year-old male immigrant from Uganda was hospitalized with protracted fevers, chest wall pain, and leukocytosis. Admission CT (**a**) revealed subtle enlargement and hypoattenuation in his right latissimus dorsi muscle (*white arrow*). Targeted US in this region revealed a complicated intramuscular fluid collection (*arrowhead*), consistent with abscess, which was successfully treated with antibiotics and ultrasound-guided percutaneous drainage (*arrow*, **b**). Gram stain and culture of the fluid grew methicillin-sensitive *Staphylococcus aureus* (MSSA)

Radiography frequently lacks adequate sensitivity for soft-tissue infection, but uncomplicated cellulitis may appear nonspecific soft-tissue swelling or fullness. Evidence of prior trauma or surgical intervention may be present. Retained radiopaque foreign bodies serve as a nidus for infection. Air-fluid levels within soft tissues on radiography often indicate abscess [42].

CT is frequently used instead of MRI given its availability and short imaging time, as well as for patients in whom MRI is contraindicated. While inferior to MRI, resolution of CT allows determination of the extent of infection and structures involved. Imaging features of soft-tissue infection on CT include hazy or indistinct soft-tissue planes with variable heterogeneous enhancement after intravenous contrast administration (Fig. 19.13). Phlegmon is defined as soft-tissue infiltration by purulent material. Abscesses represent discrete collections of pus within the soft tissues and are depicted as rim-enhancing, thick-walled, often complex, fluid collections. Percutaneous drainage procedures may be performed under CT or US guidance [41, 43, 44] (Fig. 19.12).

Fig. 19.13 Cellulitis and phlegmon. CT reveals nonspecific skin thickening and inflammatory change in the posterior soft tissues of the back in this 54-year-old diabetic patient. There is no appreciable rim enhancement to suggest abscess formation

Necrotizing Infection

Necrotizing fasciitis—a rapidly progressive deep-tissue infection—most commonly affects the perineum or abdominal wall, with rare involvement of the thorax. In most cases, chest wall-necrotizing infections occur as a complication of empyema and chest drainage procedures. Patients with these aggressive, often lethal, infections present with severe systemic infection and sepsis. Physical exam reveals dramatic chest wall pain beyond that expected by the wound's external appearance. Erythema, swelling, blistering, crepitus, and watery drainage may also be present. While no risk factors have been identified, the association of such infection is highest in patients with diabetes and other immune-compromised states [17, 45]. Most infections are polymicrobial and synergistic, with *Clostridium perfringens* and *Streptococcus* species frequently implicated. Fatal toxin release from these organisms may lead to circulatory collapse. The aggressive course of these infections explains the rate of complications, such as extension into the pleural space. Widespread involvement may also contribute to respiratory compromise and death. Rapid surgical debridement and early broad-spectrum antibiotic therapy are the mainstays of treatment. Daily debridement may be indicated until adequate source control is obtained.

Imaging features of necrotizing fasciitis are often indistinguishable from cellulitis. CT and MRI are essential in identifying deep fascial involvement or other complications of infection (vascular thrombosis, mediastinitis). CT is the most sensitive modality for the detection of deep-tissue inflammation and soft-tissue gas (Fig. 19.14). Signal voids within soft tissue on all MRI pulse sequences and areas of susceptibility on gradient echo sequences can suggest the presence of gas—a classic but variably present feature of necrotizing infection [4, 17, 42]. Importantly, the absence of soft-tissue gas does not reliably exclude necrotizing infection. Otherwise, MR findings include increased T2 signal with extension along deep fascial planes, indistinct fascial and fat planes, and tissue enhancement on T1 fat-suppressed sequences after intravenous gadolinium administration [17, 42] (Fig. 19.14). Tissue necrosis and hypoperfusion would manifest as areas of lack of enhancement.

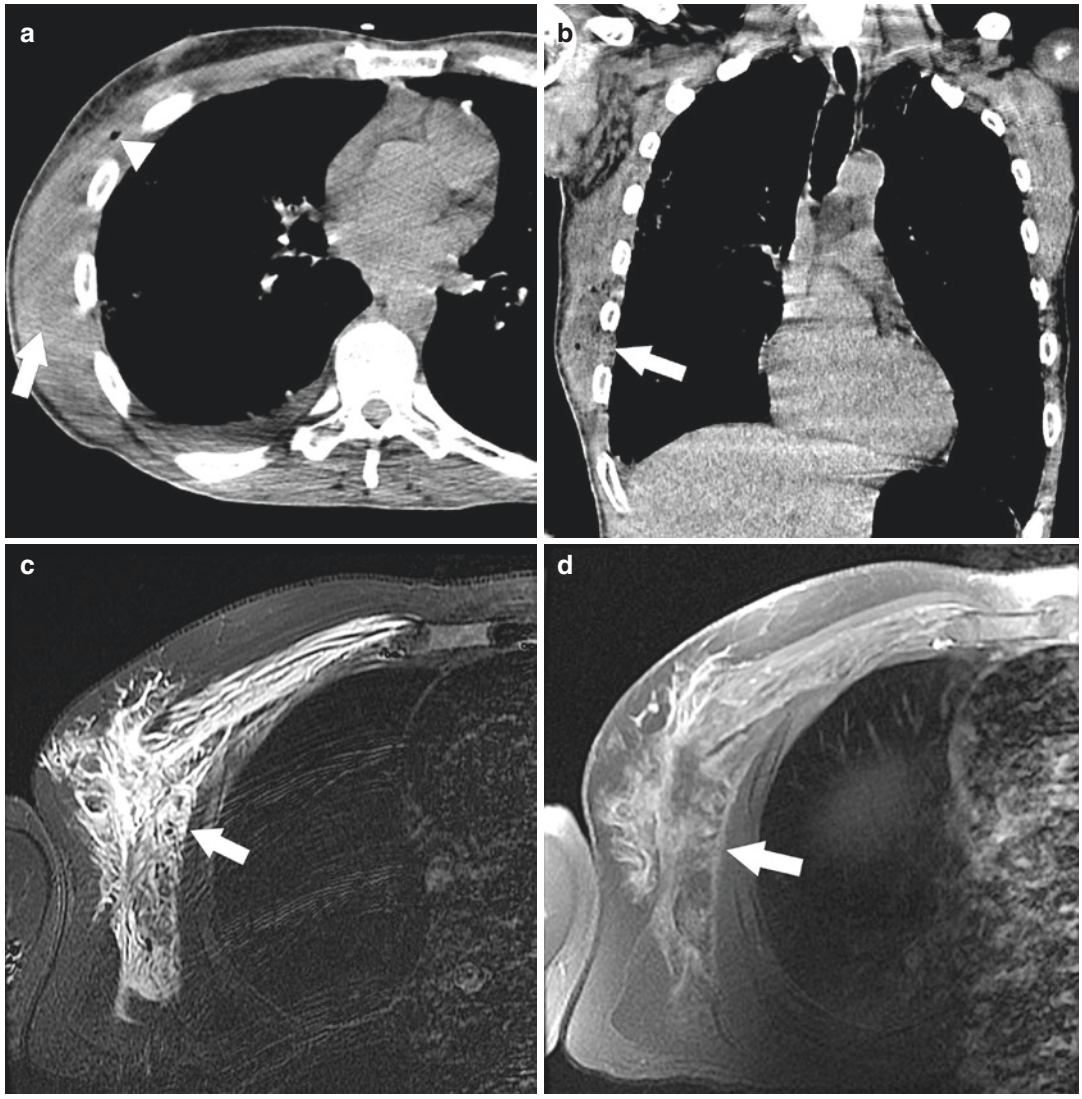

Fig. 19.14 Necrotizing fasciitis. Axial (**a**) and coronal (**b**) CT shows nonspecific soft-tissue swelling and inflammation involving the deep fascial planes in a septic, obtunded 45-year-old male with untreated HIV and IV drug use who presented with CD4 34 cells/μL and HIV PCR viral load 166 copies/mL. Bubbles of gas were present in the inflamed deep fascia (*arrowhead*). Axial STIR (**c**) and T1-weighted, fat-suppressed post-contrast (**d**) MR in a different patient who suffered extreme immunosuppression revealed extensive edema, fascial thickening, and enhancement (*arrows*, **c** and **d**) in the deep soft tissues of the right chest wall and raised concern for necrotizing infection and the patient was ultimately treated with fasciotomy

19.3 Arthritides

The chest wall architecture comprises several unique articulations, each with somewhat unique anatomic and functional features. The sternoclavicular, manubriosternal, costochondral, acromioclavicular, and glenohumeral joints are comprised of variable histologic elements and are subject to several degenerative or inflammatory diseases as in other parts of the axial and appendicular skeleton. The sternoclavicular and manubriosternal joints are often overlooked on imaging, but may come to the attention of the thoracic surgeon in the perioperative assessment

prior to sternotomy, or in patients presenting with abnormalities in these regions.

19.3.1 Osteoarthritis

The normal manubriosternal joint undergoes histologic progressive degenerative change over the life span, beginning with conversion of manubriosternal hyaline cartilage to fibrocartilage and later ossification [37]. The fibrocartilaginous components of the joint may become variably absorbed and replaced with synovial tissue. Synostoses may form when the disk ossifies, increasing in incidence with age. The second sternocostal joint is a synovial joint which contacts the lateral aspects of the manubriosternal joint. Varying degrees of joint narrowing, sclerosis, and irregularity have been described in normal manubriosternal joints.

Degenerative changes are the most common arthritic changes of the sternoclavicular and manubriosternal joints. Many radiographic and CT features are similar with the expected normal joint changes with aging, including joint space narrowing, subchondral sclerosis and cystic change, irregularity, and ankyloses [12]. Osteophyte formation and sclerosis predominate in osteoarthrosis. Intra-articular gas—the so-called—vacuum phenomenon may be detected radiographically or on CT. Similarly, patients with diffuse idiopathic skeletal hyperostosis (DISH) may demonstrate exuberant, large osteophytes and joint space flaring and wedging [37].

Lateral and oblique radiographs depict the joint to some advantage, but may be limited by rotation. Multiplanar CT in the sagittal and coronal planes is superior to radiography in depicting the joint (Fig. 19.15). Ultrasound findings of osteoarthritis of the sternoclavicular, manubriosternal, and costochondral junctions include most commonly capsular thickening, as well as echogenic marginal osteophyte and joint space narrowing [38]. Bone scintigraphy is less reliable in assessment of the sternum, as increased radiotracer uptake can be seen in non-inflamed sternoclavicular and manubriosternal joints [37]. MRI is less useful in depicting the normal anatomy of the joint, but is very sensitive to detection of bone marrow changes and surrounding soft-tissue involvement by inflammatory processes.

19.3.2 Inflammatory

19.3.2.1 Costochondritis

Costochondritis (inflammation of the costal cartilages) may be from sterile inflammation or infectious agents (*Staphylococcus, Streptococcus, Candida,* or Aspergillus species). Its incidence is increasing with the widespread abuse of IV drugs [46]. Painful chest wall abnormalities are easily evaluated with targeted ultrasound, where costochondritis may manifest as ill definition and swelling of the affected cartilage with some perichondral fluid signal (edema) [38]. Radiographic features included cartilaginous expansion, fragmentation, or adjacent bone destruction. CT findings include low attenuation of the cartilage with or without adjacent soft-tissue inflammatory changes often with localized peripheral calcification [46, 47]. Bone scintigraphy may also be used to define the extent of radiographically occult costochondritis. Tietze syndrome is a unique painful costochondritis appearing as swelling, dystrophic calcification, degenerative change, and osteophytosis of upper costochondral junctions, likely a result of recurrent anterior chest wall microtrauma.

Rheumatoid Arthritis (RA)

Imaging features of RA of the sternoclavicular and manubriosternal joints may be indistinguishable from osteoarthritis, but are generally more severe. Patients may be asymptomatic but exhibit markedly abnormal imaging findings. Typically, erosions along the articular surfaces predominate (Fig. 19.15), primarily affecting the synovium of the second sternocostal or manubriosternal joints [37]. These features are also indistinguishable from those in patients with reactive arthritis and other seronegative spondyloarthropathies. Contrast-enhanced MRI using fat-suppressed T1-weighted sequences allows for quantification of synovial volume and enhancement. MR

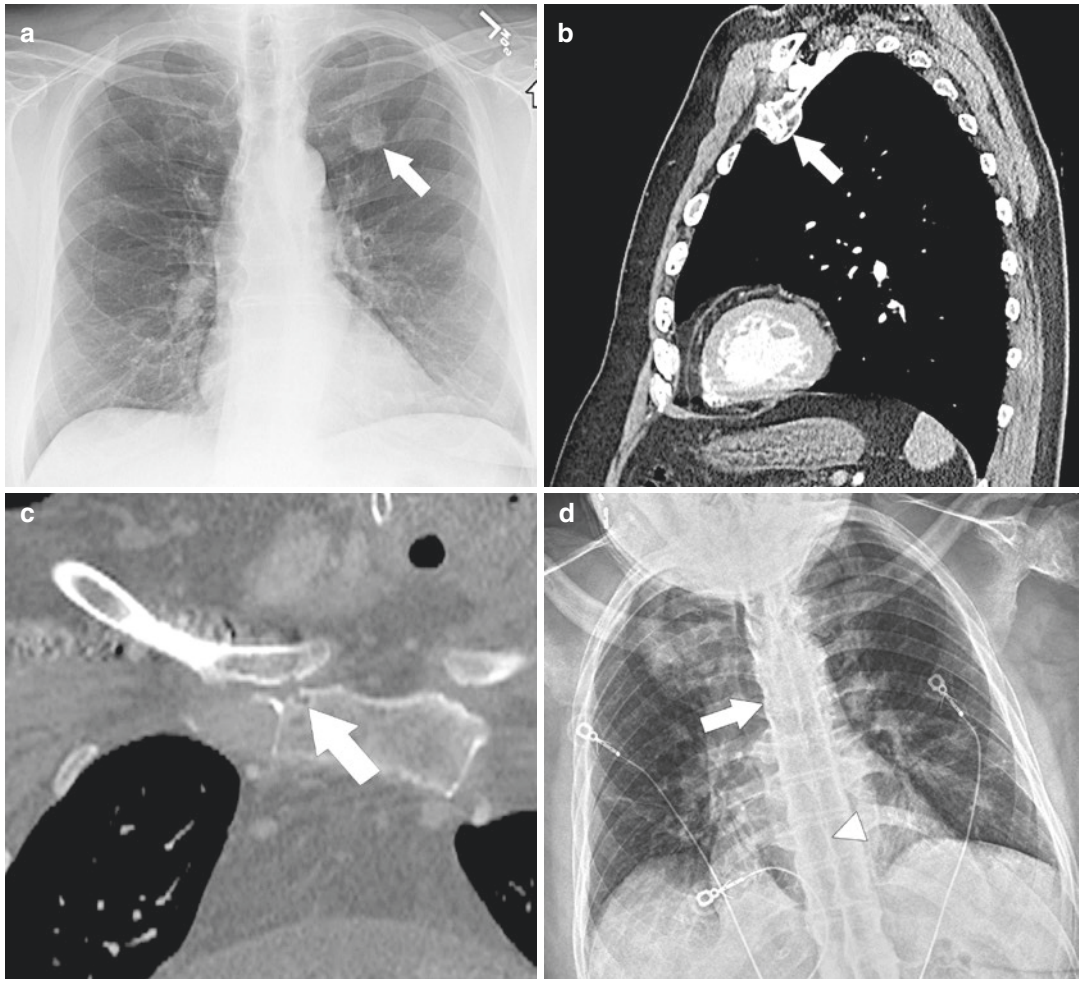

Fig. 19.15 Chest wall arthritides. (**a**) Posterior-anterior chest radiograph reveals a dense rounded opacity projecting over the left upper lung zone (*arrow*), which raised concern for an underlying lung cancer. (**b**) Sagittal contrast-enhanced CT showed no lung mass, but detailed marked degenerative osteoarthritis and osteophyte formation involving the left costochondral articulation (*arrow*). (**c**) Joint space erosion (*arrow*) and periarticular inflammation is present in the right sternoclavicular joint in the patient with long-standing rheumatoid arthritis. (**d**) Anterior–posterior chest radiograph reveals bridging syndesmophytes (*arrow*) and interspinous ligament calcification (*arrowhead*), which respectively create the "bamboo spine" and "dagger sign" radiographic descriptors associated with ankylosing spondylitis. (**e**) Sagittal CT in a different patient depicts the thin syndesmophytes (*arrow*) formed in the spine, a specific feature of ankylosing spondylitis. (**f**, **g**) Sheetlike chest wall calcifications (*arrows*) involve the deep fascia in this patient with dermatomyositis

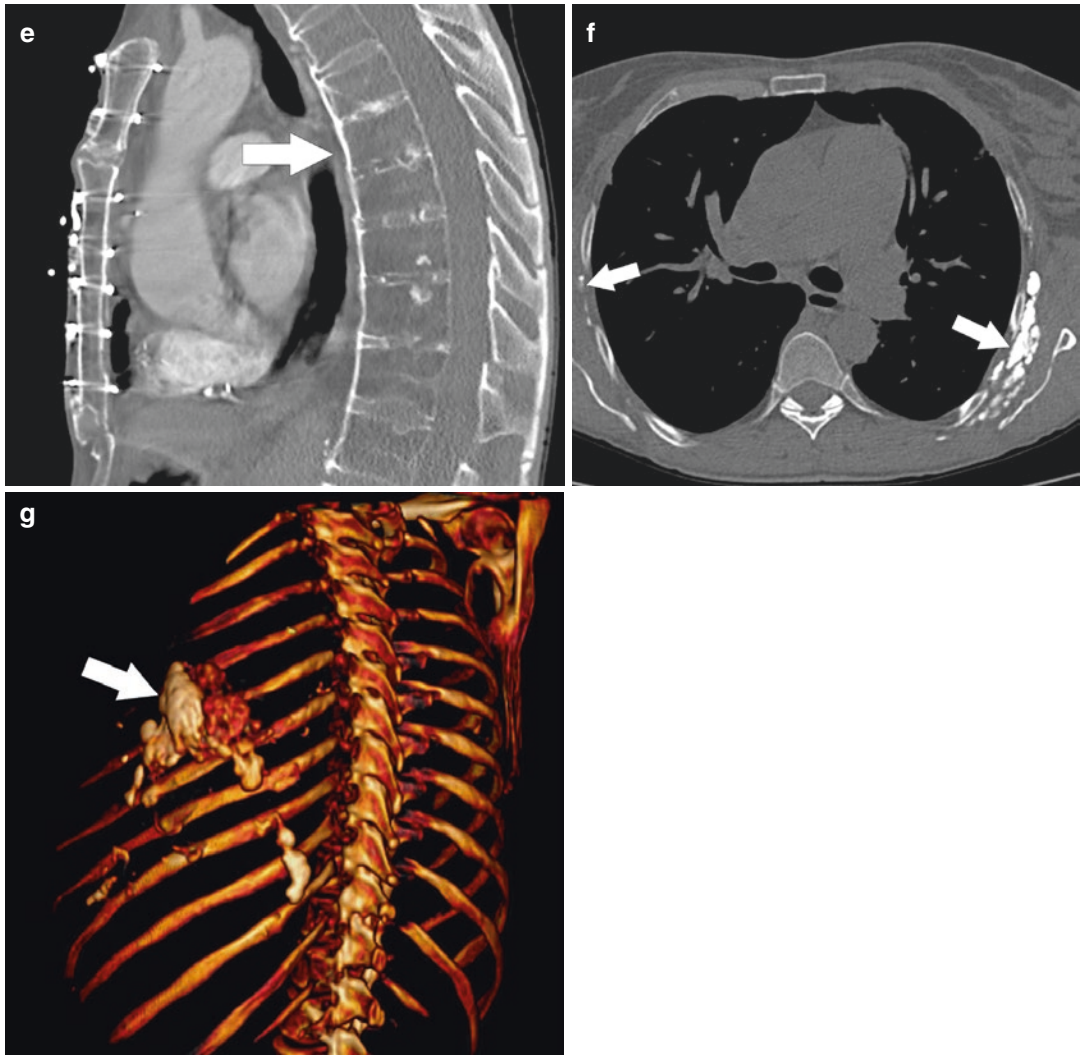

Fig. 19.15 (continued)

best depicts associated findings of bone marrow edema and enhancement [12].

Ankylosing Spondylitis, Dermatomyositis

Imaging features of ankylosing spondylitis include osseous expansion, joint erosion, and ankylosis, with ankylosis as a predominant feature [37]. Bridging syndesmophytes and ankylosis of facets are consistent features of ankylosing spondylitis (Fig. 19.15) forming a rigid spine, often referred as the bamboo spine, which is at increased risk for fractures, even from minor trauma. Fusion and erosion are the most common imaging features of psoriatic arthritis of the sternal joints, occurring in nearly 100% of cases. In addition to joint erosions, a characteristic manifestation of dermatomyositis is the formation of sheets of calcification along fascial planes (Fig. 19.15).

19.3.3 Crystalline Deposition Disease

19.3.3.1 Gout

Gout rarely affects the sternum, and imaging findings are often nonspecific, overlapping with those of degenerative change [37]. Rarely, gouty tophus may be seen. Imaging features include juxta-articular erosion and marginal bony deposition creating the classically described "overhanging edge" [12]. Acute inflammation is shown on MRI as increased periarticular T2 signal with enhancement.

19.3.3.2 Calcium Pyrophosphate Dehydrate Deposition Disease (CPPD)

CPPD may be deposited in the joint capsules of the sternum or ribs, with imaging features similar to those of osteoarthritis [37]. Calcifications within the cartilage (chondrocalcinosis) and articular disks of the sternoclavicular joints may be present on radiographs or CT. Rarely, periarticular soft-tissue calcifications (pseudogout) may be present [12].

19.4 Metabolic Disorders

19.4.1 Osteopenia and Osteoporosis

Low bone density is common among the elderly, as well as patients with predisposing conditions (inactivity, chronic inflammatory conditions, chronic renal failure, chronic corticosteroid therapy, COPD, estrogen deficiency, among others). Bone density is routinely measured with dual-energy X-ray absorptiometry (DXA) scans in at-risk populations. Loss of bony trabeculae is the histologic hallmark of osteoporosis, which leads to weakening of the bone and predisposition to insufficiency fractures. Sternal insufficiency fractures (SIF) have been described in the setting of osteoporosis, thought related to a combination of low bone mass and abnormal stresses on the sternum from exaggerated thoracic kyphosis (also found commonly in osteoporotic patients) (Fig. 19.16). Forceful coughing may also result in SIF [48–50]. Radiographic and CT evaluations classify SIF as either buckling or non-buckling based on absent cortical disruption, callus formation, or localized bone resorption in the former and posterior position of the upper part of the sternum in the latter [48] (Fig. 19.16). Non-buckling fractures are further subdivided into displaced (cortical offset of >25% of the width of the sternum on lateral radiographs) or non-displaced. Chest pain is the most common symptom at presentation. However, patients with buckling SIF are frequently asymptomatic.

19.4.2 Renal Osteodystrophy

Renal osteodystrophy refers to musculoskeletal alterations that are found in association with chronic renal insufficiency and treatments thereof, all of which involve complex metabolic alterations of calcium, phosphate, and vitamin D. Modern advances in the care related to chronic renal disease (i.e., hemodialysis and renal transplantation) have led to an increase in the incidence of these disorders on routine thoracic imaging. Radiographic manifestations classically include subperiosteal, subchondral, and subligamentous bone resorption/osteolysis which commonly occur in the sternoclavicular and acromioclavicular joints, as well as intervertebral disks and coracoclavicular ligamentous insertions [51]. Diffuse osteosclerosis results from a combination of effects from renal osteodystrophy and secondary hyperparathyroidism, frequently visualized in the axial skeleton as subendplate osteosclerosis with normal density of the middle of the vertebral body, the so-called rugger-jersey spine (Fig. 19.16). Osteoporosis is frequently found in patients with chronic renal disease, predisposing to thoracic vertebral compression fractures.

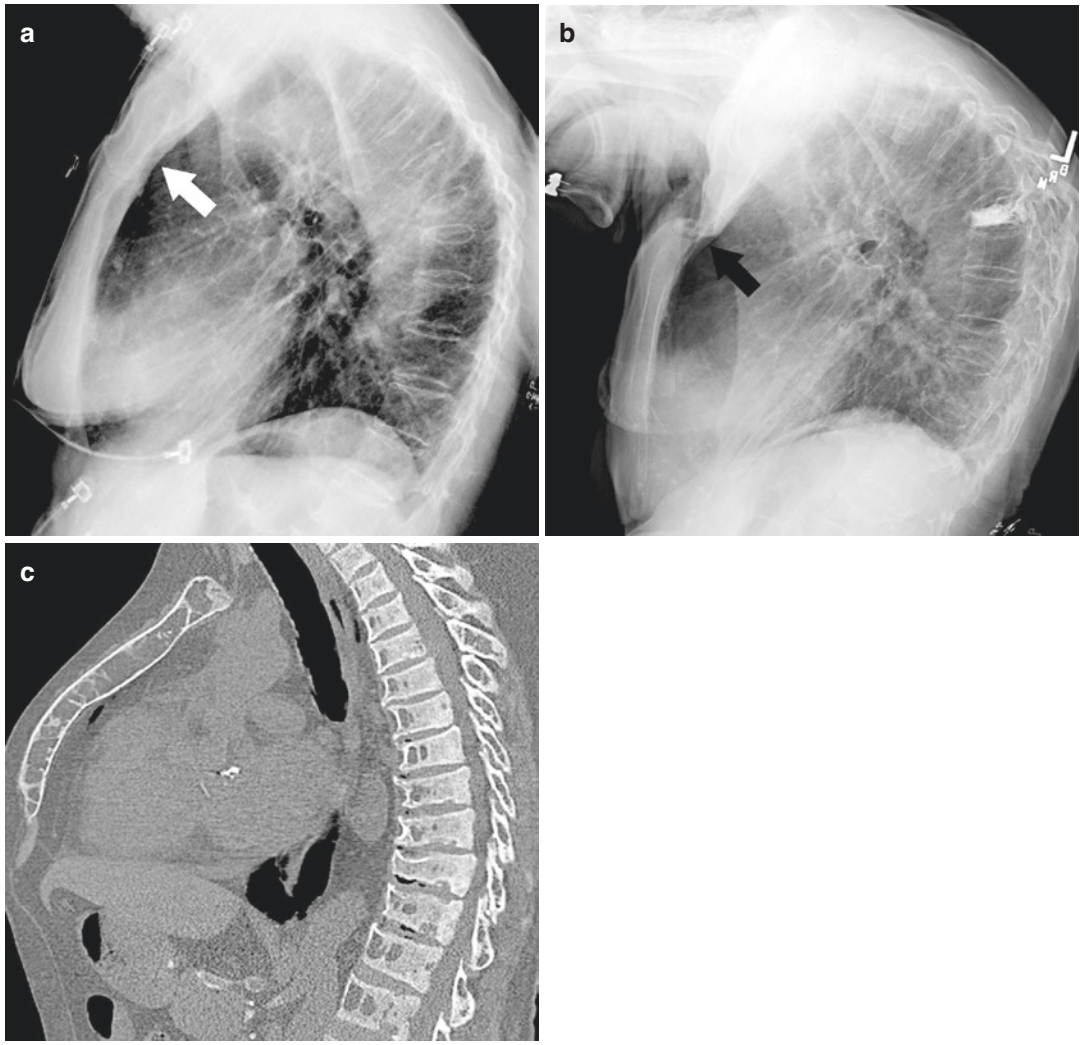

Fig. 19.16 Metabolic disorders of the chest wall. (**a**) Lateral chest radiograph in an 80-year-old patient with chest pain reveals diffuse osteopenia and an acute compression deformity of a midthoracic vertebral body. The patient's sternum is intact (*white arrow*). (**b**) Lateral chest radiograph from the same patient performed 2 years later shows vertebral augmentation of the compressed vertebral body, new compression deformities, progressive kyphosis, and development of a posteriorly displaced nonbuckling fracture of the manubrium (*black arrow*) and subtle buckling fracture of the upper sternal body. (**c**) Sagittal chest CT reveals diffuse osteosclerosis involving the vertebral bodies, as well as marrow expansion in the sternum in a patient on hemodialysis for chronic renal failure, consistent with renal osteodystrophy

19.5 Congenital

Congenital malformations of the chest wall and ribs are often found in association with spinal anomalies, most commonly scoliosis [52]. Most occur in succession of a failure of embryologic segmentation and formation of ribs from developing somites. Embryological development of the ribs, scapulae, and spine is closely linked with the scapulae and arms developing from primitive arm buds—lateral swellings along the C5 through T1 vertebral bodies during the third week of gestation. The scapulae form from the arm bud mesenchyme and migrate inferiorly to their posterolateral locations behind the second through eighth ribs.

19.5.1 Sternum

The origins of developmental anomalies of the sternum are generally regarded as sequelae either of (1) dysmorphic costal cartilage growth (pectus excavatum and pectus carinatum) or (2) an embryologic failure of the developing sternum (sternal cleft, sternal foramen, etc.).

19.5.1.1 Pectus Excavatum (Funnel Chest, Trichterbrust)

Pectus excavatum is the most common developmental sternal deformity, present in up to 1:400 live births [12, 53], with a marked male predominance of 5:1. It occurs as a result of rapid overgrowth of the lower costal cartilages, resulting in posterior displacement of the sternum and anterior positioning of the ribs. The retrosternal space is often markedly reduced with leftward displacement and rotation of the heart and reduced left lung volumes from mass effect. Pectus excavatum is often an isolated finding without a known genetic causation, but up to 45% show a familial pattern. The condition is found in association with other genetic disorders such as Marfan, Ehlers-Danlos, Loeys-Dietz, Poland, and Klippel-Feil syndromes. Also, it is not uncommon to encounter pectus excavatum in patients with bronchiectatic non-tuberculosis mycobacterial infection. Other conditions may coexist such as syndactylism, club foot, scoliosis, osteogenesis imperfecta, mitral valve prolapse, and other congenital heart diseases.

Besides the obvious cosmetic and psychological effects of pectus excavatum, there remains controversy as to the physiologic effect of sternal depression on cardiopulmonary function [12, 53]. Patients may present with exertional dyspnea, reduced exercise tolerance, angina, palpitations, wheezing, and recurrent upper respiratory infections. Pulmonary function testing (PFT) in these patients may reveal a restrictive pulmonary pattern, with diminished total lung capacity, forced vital capacity, and vital capacity—the severity of which may increase with more severe sternal depression. Several studies have suggested that exercise intolerance may be related to sternal compression, impaired filling of the right heart chambers, and reduced stroke volume [53].

The degree of sternal depression can be classified based on physical appearance as localized and symmetric (type I), diffuse and symmetric (type II), and asymmetric diffused or localized (type III). When surgery is contemplated, imaging remains a useful tool for pectus excavatum characterization and surgical planning. Chest radiographs (posteroanterior and lateral) and CT are usually sufficient. A fronto-sagittal thoracic index ("Welch index") can be measured radiographically. Others report utility of the lateral radiograph in establishment of a configuration index—a ratio of the lower vertebral index (depth of the thorax at the xiphisternal junction) and the upper vertebral index (thoracic depth at the sternomanubrial junction). CT is frequently employed for presurgical planning for pectus excavatum, with measurement of the Haller index. The Haller index is derived from an axial CT image through the deepest part of sternal depression. A ratio of the transverse thoracic diameter (width of chest between the lateral ribs) is divided by the anteroposterior diameter (anterior part of spine to lowest part of sternal depression) at the same level [53, 54]. A normal index is 2.56 ± 0.35. Ratio of more than 3.25 is associated with an increased need for operative intervention (Fig. 19.17).

19.5.1.2 Pectus Carinatum (Pigeon Breast, Chicken Breast, Pouter Chest, Pyramidal Chest)

In pectus carinatum (PC), the sternum is displaced anteriorly, and occurs five to six times less frequently than pectus excavatum. Like pectus excavatum, there is a strong male predominance, and the defect is usually isolated. However, a family history of chest wall anomalies may be present. Furthermore, pectus carinatum may coexist with cardiac anomalies and scoliosis. Patients are usually asymptomatic, but may complain of angina, exertional dyspnea, and poor exercise tolerance. The effects of pectus carinatum on pulmonary function are less clear than in pectus excavatum, but poor exercise tolerance is believed to result from

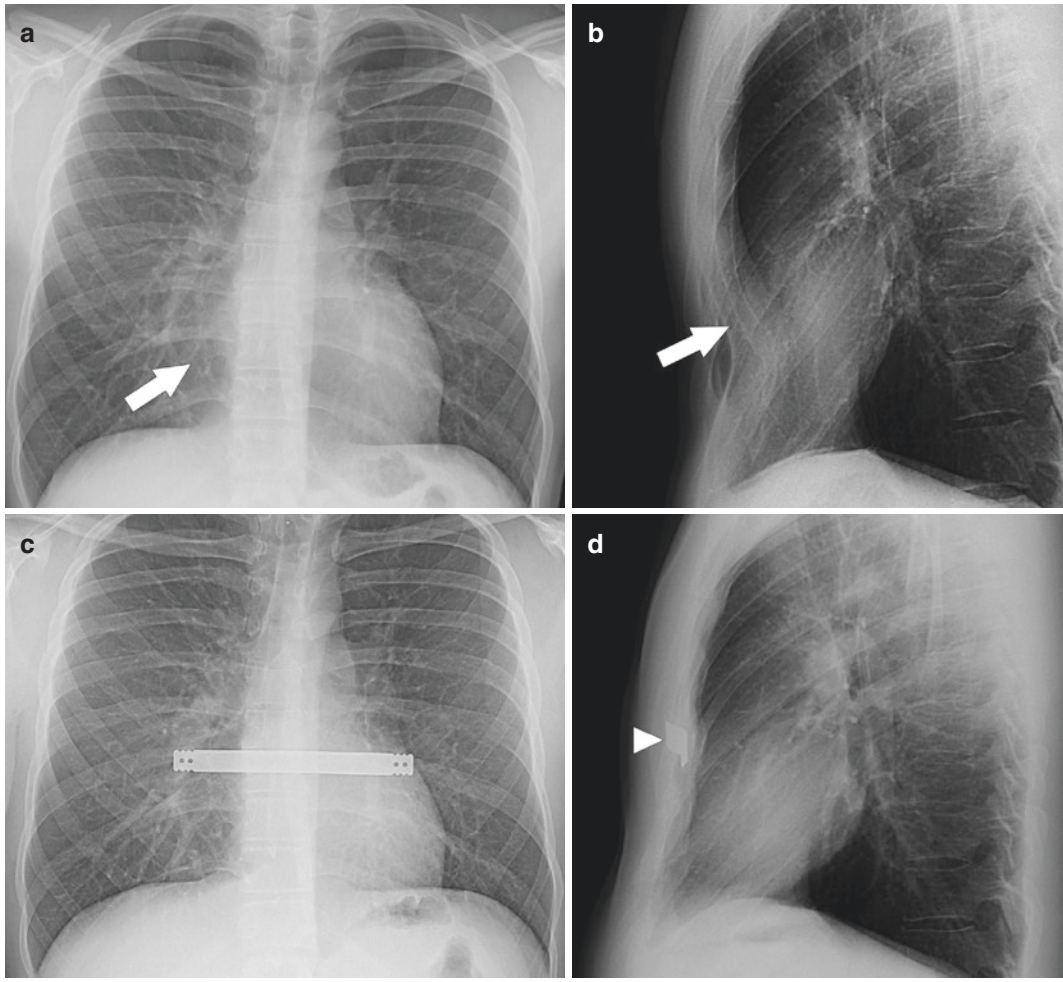

Fig. 19.17 Pectus excavatum and pectus carinatum. A 26-year-old male United States Air Force recruit presented with intermittent pleuritic anterior chest pain and dyspnea on exertion. (**a**) Posterior-anterior chest radiograph shows obscuration of the right-heart border (*arrow*), simulating right middle lobe airspace disease. (**b**) Lateral chest radiograph in the same patient shows marked xiphisternal depression with compression of the heart (*arrow*). The patient underwent subsequent Nuss procedure with placement of an Adkins strut (*arrowhead*, **d**), which improved the degree of sternal depression and mass effect on the heart (**c**, **d**). (**e**) A preoperative chest CT was performed to measure the degree of sternal depression (Haller index = 3.9). (**f**) Lateral chest radiograph depicts marked sternal protrusion (*arrow*), consistent with pectus carinatum. (**g**) Marked anterior bowing of the upper sternal body and manubriosternal joint (*arrow*) in this dyspneic 19-year-old female is consistent with the pouter chest variant of pectus carinatum.

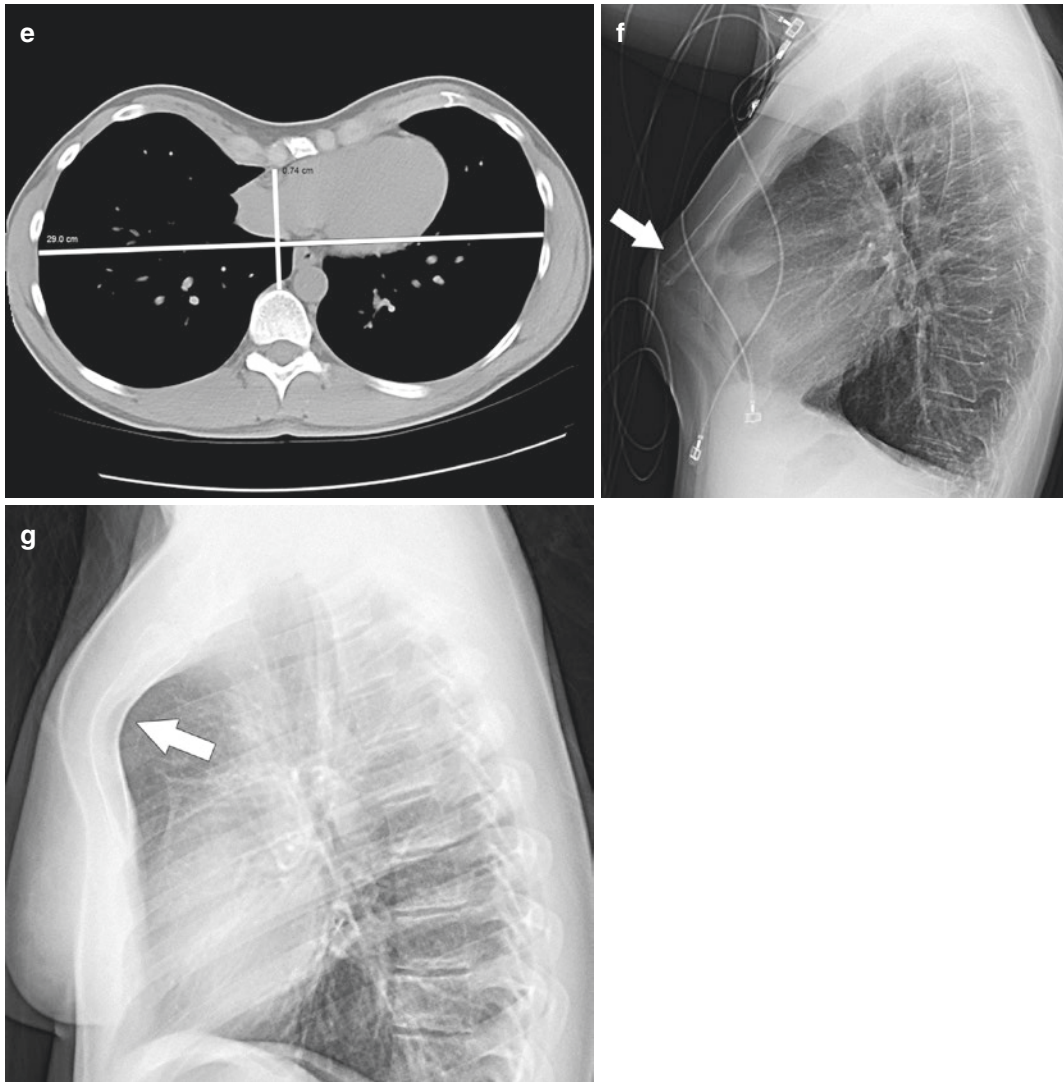

Fig. 19.17 (continued)

abnormal thoracic movement during the respiratory cycle, leading to tachypnea and diaphragmatic breathing, and eventually to fatigue [53].

A rare subtype of pectus carinatum manifests with marked enlargement and protrusion of the second costal cartilages and sternomanubrial joint (the so-called pouter chest) (Fig. 12.17). Elevation of the adjacent costal cartilages on either side of the sternomanubrial joint contributes to a U-shaped deformity of the anterior chest wall [54].

Physical examination usually reveals the defect pattern, classified as chondrogladiolar (type I, keel chest)—protrusion of the gladiolus and inferior cartilages; chondromanubrial (type II, pigeon breast)—prominence of the superior costal cartilages; and lateral PC (type III)—asymmetric deformity with unilateral sternal protrusion or rotation [53]. Chest radiography and CT can further document the severity of PC with pectus severity index of 1.2 to 2 being associated with operative repair [12].

19.5.1.3 Tilted Sternum

When the longitudinal orientation of the sternum deviates to the right or left of midline it is referred to as tilted. The resultant chest wall deformity can be found in association with anterior convex ribs or an anteriorly subluxed sternoclavicular joint [12]. Depending on the severity of tilt, these anomalies are usually incidental, and surgical consultation is usually reserved for cosmetic purposes. CT is the preferred modality for evaluation of the tilted sternum, primarily for presurgical planning and excluding underlying neoplasm as a cause for the palpable abnormality.

Sternal Bands and Clefts

The sternum is formed from enchondral ossification and midline fusion of two longitudinal bars of lateral plate mesoderm (sternal bars) oriented in a craniocaudal direction. The more common sternal band appears as a line of sclerosis along the midline embryologic cleavage plane and is usually of no clinical significance (Fig. 19.18). Bands may be seen in association with sternal clefts, which are midline defects in the sternum from failure of osseous fusion. Seventy-five percent of sternal clefts were found in female subjects in one large series [53]. Unlike bands, sternal clefts are more often found in association with other congenital abnormalities such as ectopia cordis and pentalogy of Cantrell. Clefts may result in paradoxical movement of the chest during respiration, which some believe to contribute to symptoms of dyspnea, cyanosis, and recurrent pneumonia, which justifies their frequent surgical repair. Sternal bands and clefts may be found in any part of the sternum, except that bands are not found in the xiphoid process. Axial and coronal CT best characterizes these anomalies as incomplete or complete, and their associations with orthotopic heart and ectopia cordis, respectively. Sternal clefts may rarely be seen in association with various vascular malformations such as craniofacial hemangioma, aneurysm of the ascending thoracic aorta, or obliteration of the brachiocephalic artery.

Sternal Foramen

Sternal foramina are found in 5% of the population, and appear as a "bow-tie" osseous defect on axial CT [12] (Fig. 19.18). Associated sternal bands and clefts may also be present. Radiologists should alert surgeons to the presence of sternal foramina in patients who may undergo sternal intervention (e.g., interosseous access or bone marrow aspiration) as fatal hemorrhage and cardiac tamponade may result.

19.5.1.4 Episternal Ossicles

Supernumerary ossification centers about the manubrium may result in the presence of unilateral or bilateral, pyramid-shaped accessory bones, usually 2–15 mm in size (Fig. 19.18). These are detected in 1.5% of the population, and most commonly found on CT [12]. These should be differentiated from mimics such as atherosclerotic vascular calcifications, calcified lymph nodes, fractures, and foreign bodies. As other bones, they typically exhibit a well-defined and sclerotic cortex.

19.5.2 Ribs

Rib anomalies may be classified as *simple* or *complex* relative to the extent and number of rib fusions, rib absence, chest wall defects, or general pattern of rib anomalies [52]. Most rib anomalies are simple (80%), manifest as localized fusion of 2–3 ribs. Complex rib anomalies frequently coincide with large chest wall defects. Rib anomalies are found in nearly 20% of patients with congenital deformities of the spine, and occur more commonly in females (2.5:1). Both simple and complex rib anomalies tend to occur on the concave side of associated thoracic or thoracolumbar scoliosis, most commonly associated with unilateral vertebral segmentation failure. Early detection of rib anomalies is important, as such deformities might lead to scoliotic curve progression and may assist in early planning of prophylactic treatment for these patients.

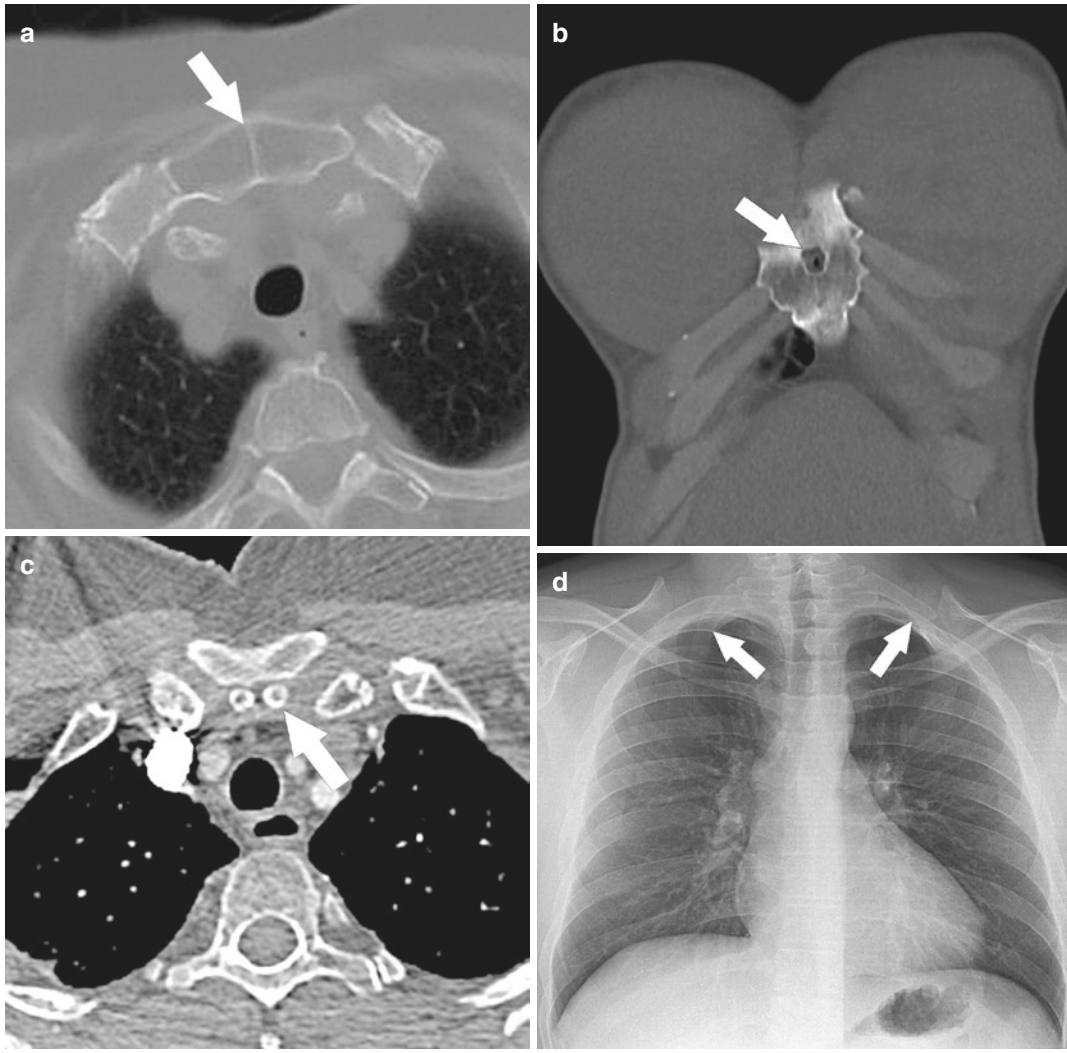

Fig. 19.18 Congenital chest wall deformities. (**a**) Incidentally detected sternal band on CT shows a line of sclerosis along the embryologic fusion plane. (**b**) Variably sized sternal foramina (*arrow*) are common. The presence of a sternal foramen should be known prior to intraosseous access or bone marrow aspiration procedures to prevent life-threatening cardiac injury. (**c**) Episternal ossicles (*arrow*) are normal structures occasionally seen near the manubrium on routine chest CT, and are of no clinical significance, but may simulate other processes. (**d**) Variably sized supernumerary (cervical) ribs (*arrows*) may be found incidentally on routine chest imaging, but can occasionally contribute to symptoms of thoracic outlet syndrome, which may require surgical intervention. (**e**) Coronal MIP and (**f**) 3D volume-rendered contrast-enhanced CT delineates extensive right shoulder venous collaterals from chronic compression of the right subclavian vein (*arrows*). (**g**) Frontal chest radiograph depicts complete absence of the clavicles (*arrows*) in this patient with cleidocranial dysostosis. (**h**) Asymmetric elevation of the right scapula (*arrow*) was detected incidentally in this patient with Sprengel deformity. An omovertebral fibro-osseous connection, though classically described, was absent in this patient and is only present in 25% of cases. (**i**) Complete absence of the right pectoral muscle (*arrow*) was detected on chest CT in this patient with Poland syndrome

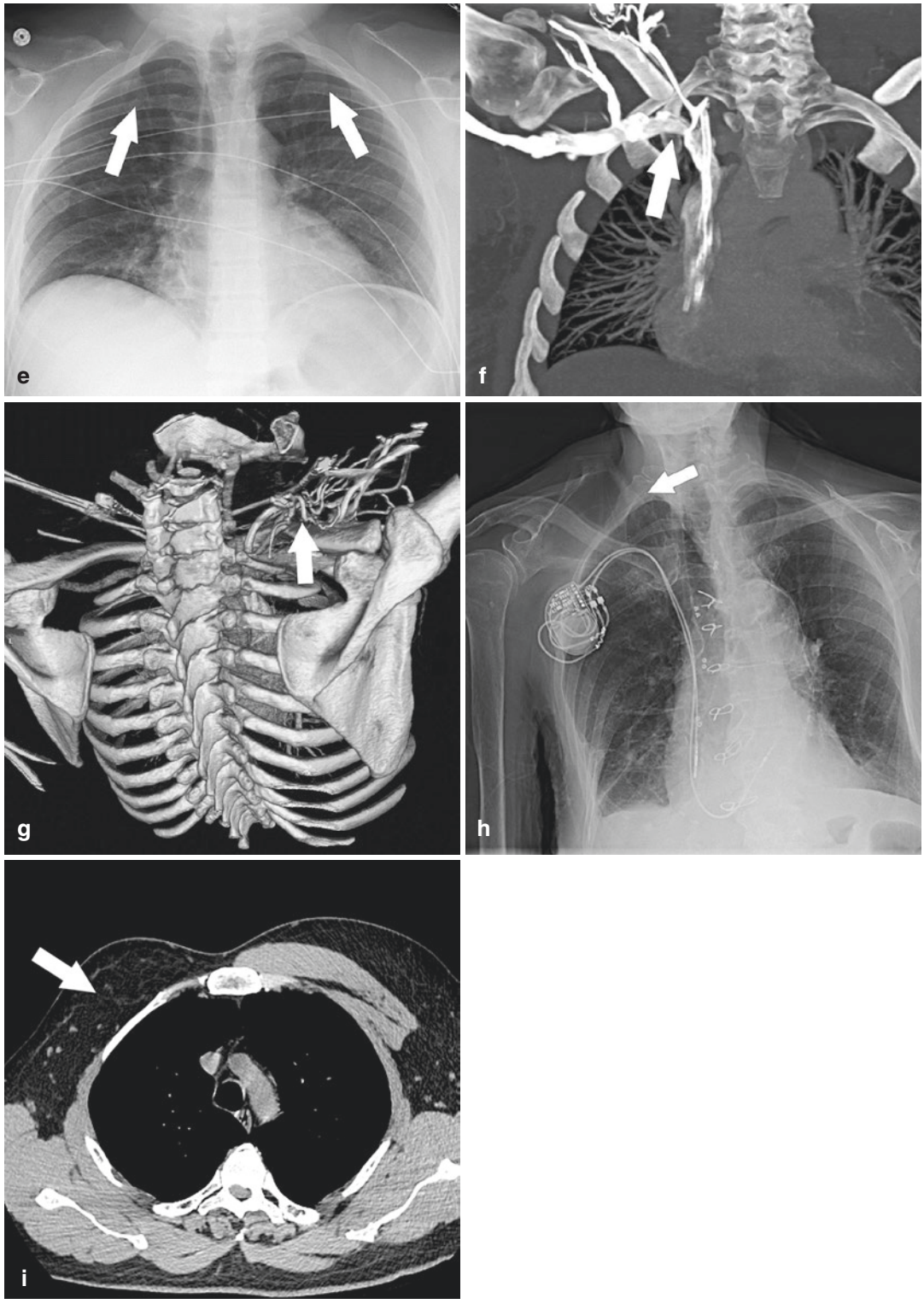

Fig. 19.18 (continued)

Cervical rib (anomalous accessory rib, "Eve's rib"). Supernumerary ribs may develop from the C7 vertebrae, and are defined as the presence of a rib with a distinct articulation with a horizontally oriented (cervical type) transverse process. The size of the rib is variable, and larger ribs may cause thoracic outlet syndrome from compression of the neurovascular structures along the thoracic outlet, leading to symptoms of arm pain and weakness, hand swelling, and positional variation in pulse intensity between the upper extremities. Cervical ribs may be detected on chest radiography and must be distinguished as supernumerary by identification of the true second rib and its reliable anterior articulation with the manubriosternal junction (Fig. 19.18). CT angiography can provide noninvasive anatomic detail related to thoracic outlet anatomy and anomalous rib (Fig. 19.18). Dynamic fluoroscopic angiography and Doppler US can document compression of the subclavian artery by the cervical rib between upper extremity adduction and abduction, confirming the diagnosis [19, 55].

19.5.3 Clavicle

Cleidocranial dysostosis Cleidocranial dysostosis is the most common congenital anomaly of the clavicle. It manifests as incomplete ossification, with associated defects in vertebral, long bone, and pubic bone development. The clavicles are usually underdeveloped, with residual hypoplastic segments, but may be completely absent [19, 56] (Fig. 19.18).

19.5.4 Scapulae

Sprengel deformity. Congenital elevation of the scapula (Sprengel deformity) is a rare consequence of congenital interruption in the caudal descent of the scapula in early development. The presence of an omovertebral fibro-osseous connection between the cervical spine and scapula is classically associated, occurring in 20–25% of cases. A hypoplastic, elevated scapula (Fig. 19.18) results in altered range of motion to the affected extremity in addition to cosmetic consequences that may worsen with continued growth of the child [57]. Sprengel deformity may be seen in association with other vertebral and rib anomalies, and is present in 20-42% of patients with Klippel-Feil syndrome [58]. This condition is generally surgically repaired early in life (2–5 years) using various techniques. The degree of scapular deformity may be graded radiographically using the Rigault classification, using the craniocaudal position of the superomedial angle of the clavicle on AP radiographs. The deformity is considered grade 1 when the superomedial angle of the scapula projects above the T4 transverse process, grade 2 when located between C5 and T2, and grade 3 when positioned above C5 [57, 59]. 3D CT reformations may assist the surgeon in preoperative planning.

19.5.5 Soft Tissues

19.5.5.1 Poland Syndrome

Rarely, the sternal portion of the pectoralis major muscle may be congenitally absent or hypoplastic from failed mesodermal development in a quadrant of the fetus, the so-called Poland syndrome. The clavicular portion of the pectoralis muscle is typically spared. The anomaly is most commonly right sided. Other associations in this syndrome include ipsilateral syndactyly, ipsilateral simian crease, aplastic ipsilateral breast tissue, absence or hypoplasia of the pectoralis minor muscle, and absence or hypoplasia of the ipsilateral second through fifth ribs [19]. Relative hyperlucency of the affected hemithorax is found on chest radiography, while CT better defines the extent of musculoskeletal involvement [54] (Fig. 19.18).

Conclusion

Nonneoplastic chest wall lesions often come to the attention of the thoracic surgeon. Comprehensive imaging of any chest wall lesion is integral to lesion characterization, detection of concomitant intrathoracic conditions, and direction of operative or nonoperative patient management.

References

1. Lomoschitz FM, Eisenhuber E, Linnau KF, Peloschek P, Schoder M, Bankier AA. Imaging of chest trauma: radiological patterns of injury and diagnostic algorithms. Eur J Radiol. 2003;48:61–70. https://doi.org/10.1016/S0720-048X(03)00202-X.
2. Battle C, Hutchings H, Evans PA. Blunt chest wall trauma: a review. Dent Traumatol. 2013;15:156–75. https://doi.org/10.1177/1460408613488480.
3. Sangster GP, González-Beicos A, Carbo AI, Heldmann MG, Ibrahim H, Carrascosa P, Nazar M, D'Agostino HB. Blunt traumatic injuries of the lung parenchyma, pleura, thoracic wall, and intrathoracic airways: multidetector computer tomography imaging findings. Emerg Radiol. 2007;14:297–310. https://doi.org/10.1007/s10140-007-0651-8.
4. Lee TJ, Collins J. MR imaging evaluation of disorders of the chest wall. Magn Reson Imaging Clin N Am. 2008;16:355–79. https://doi.org/10.1016/j.mric.2008.03.001.
5. Palas J, Matos AP, Mascarenhas V, Herédia V, Ramalho M. Multidetector computer tomography: evaluation of blunt chest trauma in adults. Radiol Res Pract. 2014;2014:1–12. https://doi.org/10.1155/2014/864369.
6. Peters S, Nicolas V, Heyer CM. Multidetector computed tomography-spectrum of blunt chest wall and lung injuries in polytraumatized patients. Clin Radiol. 2010;65:333–8. https://doi.org/10.1016/j.crad.2009.12.008.
7. Rainer TH, Griffith JF, Lam E, Lam PKW, Metreweli C. Comparison of thoracic ultrasound, clinical acumen, and radiography in patients with minor chest injury. J Trauma Inj Infect Crit Care. 2004;56:1211–3. https://doi.org/10.1097/01.TA.0000075800.65485.48.
8. Turk F, Kurt AB, Saglam S. Evaluation by ultrasound of traumatic rib fractures missed by radiography. Emerg Radiol. 2010;17:473–7. https://doi.org/10.1007/s10140-010-0892-9.
9. Nummela, M.. The incidence and effect on mortality of costochondral fractures in blunt polytrauma patients-a review of 1461 consecutive whole body CT studies for trauma. Radiological Society of North America 2016 Scientific Assembly and Annual Meeting, Chicago, IL; 2016. archive.rsna.org/2016/16002567.html.
10. Melenevsky Y, Yablon CM, Ramappa A, Hochman MG. Clavicle and acromioclavicular joint injuries: a review of imaging, treatment, and complications. Skeletal Radiol. 2011;40:831–42. https://doi.org/10.1007/s00256-010-0968-3.
11. Groves CJ, Cassar-Pullicino VN, Tins BJ, Tyrrell PNM, McCall IW. Chance-type flexion-distraction injuries in the thoracolumbar spine: MR imaging characteristics. Radiology. 2005;236:601–8. https://doi.org/10.1148/radiol.2362040281.
12. Restrepo CS, Martinez S, Lemos DF, Washington L, McAdams HP, Vargas D, Lemos JA, Carrillo JA, Diethelm L. Imaging appearances of the sternum and sternoclavicular joints. Radiographics. 2009;29:839–59. https://doi.org/10.1148/rg.293055136.
13. O'Brien SD, Bui-Mansfield LT. Costovertebral fracture dislocations: important radiographically difficult diagnosis. J Comput Assist Tomogr. 2009;33:748–51.
14. Kishen TJ, Mohapatra B, Diwan AD, Etherington G. Post-traumatic thoracic scoliosis with rib head dislocation and intrusion into the spinal canal: a case report and review of literature. Eur Spine J. 2010;19:183–6. https://doi.org/10.1007/s00586-010-1321-1.
15. Nguyen BM, Plurad D, Abrishami S, Neville A, Putnam B, Kim DY. Utility of chest computed tomography after a "normal" chest radiograph in patients with thoracic stab wounds. Am Surg. 2015;81:965–8.
16. McCarthy EF, Sundaram M. Heterotopic ossification: a review. Skeletal Radiol. 2005;34:609–19. https://doi.org/10.1007/s00256-005-0958-z.
17. Hayeri MR, Ziai P, Shehata ML, Teytelboym OM, Huang BK. Soft-tissue infections and their imaging mimics: from cellulitis to necrotizing fasciitis. Radiographics. 2016;36:1888–910. https://doi.org/10.1148/rg.2016160068.
18. Kuhlman JE, Bouchardy L, Fishman EK, Zerhouni EA. CT and MR imaging evaluation of chest wall disorders. Radiogr Rev Publ Radiol Soc N Am Inc. 1994;14:571–95. https://doi.org/10.1148/radiographics.14.3.8066273.
19. Jeung MY, Gangi A, Gasser B, Vasilescu C, Massard G, Wihlm JM, Roy C. Imaging of chest wall disorders. Radiogr Rev Publ Radiol Soc N Am Inc. 1999;19:617–37. https://doi.org/10.1148/radiographics.19.3.g99ma02617.
20. Restrepo CS, Giménez CR, McCarthy K. Imaging of osteomyelitis and musculoskeletal soft tissue infections: current concepts. Rheum Dis Clin North Am. 2003;29:89–109.
21. Blasberg JD, Donington JS. Infections and Radiation Injuries Involving the Chest Wall. Thorac Surg Clin. 2010;20:487–94. https://doi.org/10.1016/j.thorsurg.2010.06.003.
22. Chelli Bouaziz M, Jelassi H, Chaabane S, Ladeb MF, Ben Miled-Mrad K. Imaging of chest wall infections. Skeletal Radiol. 2009;38:1127–35. https://doi.org/10.1007/s00256-008-0636-z.
23. Elahi MM, Mitra A, Spears J, Tariq GB, McClurken JB. Aspergillus chest wall osteomyelitis: surgical and medical management. Eur J Plast Surg. 2004;26:425–9. https://doi.org/10.1007/s00238-003-0584-8.
24. Pineda C, Vargas A, Rodríguez AV. Imaging of osteomyelitis: current concepts. Infect Dis Clin North Am. 2006;20:789–825. https://doi.org/10.1016/j.idc.2006.09.009.
25. Hsu P-K, Hsu W-H. Chest wall mass caused by salmonella enteritidis-a pitfall of pet imaging interpretation. Thorac Cardiovasc Surg. 2008;56:239–40.
26. Varanauskienė E, Mašanauskienė E. Tuberculosis complications after bcg treatment for urinary bladder cancer. Med Kaunas. 2012;48:563–5.

27. Gözübüyük A, Özpolat B, Gürkök S, Çaylak H, Yücel O, Kavaklı K, Dakak M, Genç O. Surgical management of chest wall tuberculosis. J Cutan Med Surg. 2009;13:33–9. https://doi.org/10.2310/7750.2008.07084.
28. Saifudheen K, Anoop TM, Mini PN, Ramachandran M, Jabbar PK, Jayaprakash R. Primary tubercular osteomyelitis of the sternum. Int J Infect Dis. 2010;14:e164–6. https://doi.org/10.1016/j.ijid.2009.03.021.
29. Grover SB, Jain M, Dumeer S, Sirari N, Bansal M, Badgujar D. Chest wall tuberculosis - a clinical and imaging experience. Indian J Radiol Imaging. 2011;21:28–33. https://doi.org/10.4103/0971-3026.76051.
30. Catano J, Perez J. Tuberculosis abscess of the chest wall. Am J Trop Med Hyg. 2014;91:663. https://doi.org/10.4269/ajtmh.14-0063.
31. Lopez-Menendez C, Ruiz-Martinez R, Molino-Trinidad C, et al. Pulmonary actinomycosis with thoracic soft tissue mass: a rare onset form. Eur J Radiol. 2001;37:195–9.
32. Yeung VHW, Wong QHY, Chao NSY, Leung MWY, Kwok WK. Thoracic actinomycosis in an adolescent mimicking chest wall tumor or pulmonary tuberculosis. Pediatr Surg Int. 2008;24:751–4. https://doi.org/10.1007/s00383-008-2155-3.
33. Walker WA, Pate JW. Primary Aspergillus osteomyelitis of the sternum. Ann Thorac Surg. 1991;52:868–70.
34. Boudaya M-S, Mlika M, Chaari Z, Zribi H, Aouadi S, Marghli A, Kilani T. Chest wall hydatidosis: A single institution experience. Arch Clin Infect Dis. 2016;11. https://doi.org/10.5812/archcid.35134.
35. Topuzlar M, Eken C, Ozkurt B, Khan F. Possible anaphylactic reaction due to pulmonary hydatid cyst rupture following blunt chest trauma: a case report and review of the literature. Wilderness Environ Med. 2008;19:119. https://doi.org/10.1580/07-WEME-CR-1561.1.
36. Tanaka Y, Kato H, Shirai K, Nakajima Y, Yamada N, Okada H, Yoshida T, Toyoda I, Ogura S. Sternoclavicular joint septic arthritis with chest wall abscess in a healthy adult: a case report. J Med Case Reports. 2016;10. https://doi.org/10.1186/s13256-016-0856-0.
37. Ehara S. Manubriosternal joint: imaging features of normal anatomy and arthritis. Jpn J Radiol. 2010;28:329–34. https://doi.org/10.1007/s11604-010-0438-9.
38. Lee RKL, Griffith JF, Ng AWH, Sitt JCM. Sonography of the chest wall: a pictorial essay: sonography of the chest wall. J Clin Ultrasound. 2015;43:525–37. https://doi.org/10.1002/jcu.22286.
39. Gorospe L, Ayala-Carbonero AM, Rodríguez-Díaz R, García Latorre R, Muñoz-Molina GM, Cabañero-Sánchez A. Tuberculosis of the manubriosternal joint and concurrent asymptomatic active pulmonary tuberculosis in a patient presenting with a chest wall mass. Clin Imaging. 2015;39:311–4. https://doi.org/10.1016/j.clinimag.2014.08.006.
40. Sallés M, Olivé A, Perez-Andres R, Holgado S, Mateo L, Riera E, Tena X. The SAPHO syndrome: a clinical and imaging study. Clin Rheumatol. 2011;30:245–9. https://doi.org/10.1007/s10067-010-1560-x.
41. Kroshinsky D, Grossman ME, Fox LP. Approach to the patient with presumed cellulitis. Semin Cutan Med Surg. 2007;26:168–78. https://doi.org/10.1016/j.sder.2007.09.002.
42. Turecki MB, Taljanovic MS, Stubbs AY, Graham AR, Holden DA, Hunter TB, Rogers LF. Imaging of musculoskeletal soft tissue infections. Skeletal Radiol. 2010;39:957–71. https://doi.org/10.1007/s00256-009-0780-0.
43. Bailey E, Kroshinsky D. Cellulitis: diagnosis and management. Dermatol Ther. 2011;24:229–39.
44. Swartz MN. Cellulitis. N Engl J Med. 2004;350:904–12.
45. Birnbaum DJ, D'Journo XB, Casanova D, Thomas PA. Necrotizing fasciitis of the chest wall. Interact Cardiovasc Thorac Surg. 2010;10:483–4. https://doi.org/10.1510/icvts.2009.222323.
46. Meyer CA, White CS. Cartilaginous disorders of the chest. Radiographics. 1998;18:1109–23.
47. Ontell FK, Moore EH, Shepard JA, Shelton DK. The costal cartilages in health and disease. Radiogr Rev Publ Radiol Soc N Am Inc. 1997;17:571–7. https://doi.org/10.1148/radiographics.17.3.9153697.
48. Chen C, Chandnani V, Kang HS, Schils JP, Resnick D, Bjorkengren AG, Kaplan P. Insufficiency fracture of the sternum caused by osteopenia: plain film findings in seven patients. AJR Am J Roentgenol. 1990;154:1025–7.
49. Cooper KL. Insufficiency fractures of the sternum: a consequence of thoracic kyphosis? Radiology. 1988;167:471–2. https://doi.org/10.1148/radiology.167.2.3357957.
50. Min J-K, Sung M-S. Insufficiency fractures of the sternum. Scand J Rheumatol. 2003;32:179–80.
51. Degrassi F, Quaia E, Martingano P, Cavallaro M, Cova MA. Imaging of haemodialysis: renal and extrarenal findings. Insights Imaging. 2015;6:309–21. https://doi.org/10.1007/s13244-015-0383-3.
52. Tsirikos AI, McMaster MJ. Congenital anomalies of the ribs and chest wall associated with congenital deformities of the spine. J Bone Joint Surg Am. 2005;87:2523–36. https://doi.org/10.2106/JBJS.D.02654.
53. McGuigan RM, Azarow KS. Congenital chest wall defects. Surg Clin North Am. 2006;86:353–70. https://doi.org/10.1016/j.suc.2005.12.012.
54. Colombani PM. Preoperative assessment of chest wall deformities. Semin Thorac Cardiovasc Surg. 2009;21:58–63. https://doi.org/10.1053/j.semtcvs.2009.04.003.
55. Chang KZ, Likes K, Davis K, Demos J, Freischlag JA. The significance of cervical ribs in thoracic outlet syndrome. J Vasc Surg. 2013;57:771–5. https://doi.org/10.1016/j.jvs.2012.08.110.

56. Kumar R, Madewell JE, Swischuk LE, Lindell MM, David R. The clavicle: normal and abnormal. Radiographics. 1989;9:677–706.
57. Andrault G, Salmeron F, Laville JM. Green's surgical procedure in Sprengel's deformity: Cosmetic and functional results. Orthop Traumatol Surg Res. 2009;95:330–5. https://doi.org/10.1016/j.otsr.2009.04.015.
58. Radmore L, Thomas W, Tasker A, Diamond D, Amirfeyz R, Gargan M. Sprengel's deformity. Orthop Trauma. 2011;25:131–4.
59. Bhatia D, DasGupta B, Kadavkolan A, Bhosale P. Sprengel′s deformity of the shoulder: Current perspectives in management. Int J Shoulder Surg. 2011;5(1). https://doi.org/10.4103/0973-6042.80459.